



Understanding the Effect of Calcination Process on the Mesoporous MCM-41 Material Morphology

Rahmiye Zerrin Yarbay Şahin^{1,2*}  

¹Bilecik Şeyh Edebali University Department of Chemical Engineering, 11210 Bilecik, Turkey

²Bilecik Şeyh Edebali University Energy Technologies Application and Research Centre, 11210 Bilecik, Turkey

The pore structure, which is known to be affected by calcination, is one of the desired features for materials especially when considered to be catalysts. The improvement in the structure occurs after removing all template ions during the calcination process. This study attempts to evaluate the impact of the calcination process on properties of mesoporous MCM-41 (Mobile Composition of Matter 41) obtained via sol-gel method. Characterization of calcined and untreated samples was performed by N₂ adsorption-desorption, scanning electron microscopy (SEM) and Fourier transform infrared spectroscopy (FT-IR) analysis. The results showed that the calcination process displayed a significant impact on the MCM-41 materials. After calcination, the MCM-41 sample possessed higher surface area and smaller pore diameter, compared to the untreated one. Finally, the calcination acted as an effective pore modulating procedure, thus giving a significant impact on the morphology of the studies of MCM-41. Therefore, the calcination step in MCM-41 material preparation is explained in detail ensuring valuable characterization information to the literature.

Keywords: Calcination effect; MCM-41; Sol-gel method; Uncalcined MCM-41.

Submitted: June 08, 2021. **Accepted:** July 12, 2021.

Cite this: Yarbay Şahin RZ. Understanding the Effect of Calcination Process on the Mesoporous MCM-41 Material Morphology. JOTCSB. 2021;4(2):27-32.

***Corresponding Author. E-mail:** zerrin.yarbay@bilecik.edu.tr

INTRODUCTION

Since porous materials are popular due to the ability to network with atoms, ions, and molecules, ordered mesoporous materials have gained great attention in science since 1992 (1). Among these materials, MCM-41 (Mobile Composition of Matter 41) which has a hexagonal array of uniformly sized one-dimensional pore geometry (2). Owing to their advantages like large specific surface areas and well-defined pore structures, these materials are ideal for many areas such as adsorption, separation, energy, and drug delivery systems. Among the applications, the most popular use of porous materials is the one that can be defined as a catalytic material. Therefore, the entrance of the heteroatoms inside these materials to make them catalytically active could result to a diminution in

the quality of the pore structure that could add onto the synthesis and calcination parameters (3).

Crystalline products with varied compositions, structures, and morphologies could be attained by altering the calcination conditions such as temperature, duration, and heating rate (4). As calcination is known as an endothermic reaction, temperature in the calcination zone of the particle declines and a heat transfer which is significantly affected by particle size arises from the particle surroundings to the relevant zone (5).

Although many studies deal with MCM-41 synthesis in terms of factors such as different synthesis methods (6-8), calcination temperature (9), and calcination atmosphere (10,11). Martínez-Edo et al. published a comprehensive paper related to synthesis and applications of MCM-41 in catalysis.

They reviewed some catalytic systems using mono and di-functionalized MCM-41 as basic and acidic catalysts based on metallic complexes supported by MCM-41, metallic nanoparticles embed onto functionalized MCM-41 and magnetic MCM-41. They underlined that although the supports like SBA-15, MCM-41 are cheap, synthetically versatile, and can be reused, an advantage over other systems is that MCM-41 have been extensively studied due to their applications in biological applications. Furthermore, the chemical versatility of MCM-41 relies not only on the easy preparation of the molecular sieves, but also on the straightforward regioselective functionalization, both within the inner walls of the pores and the outside surface of the particle (12). Wu et al. studied graded synthesis of highly ordered MCM-41 and carbon/zeolite composite from coal gasification fine residue for crystal violet removal. They found that MCM-41 with large BET of 1013 m²/g exhibited five characteristics diffraction peaks. They stated that the common silicon sources like ethyl orthosilicate (TEOS) or sodium metasilicate are of high cost. Therefore, cheap solid waste as an alternative raw material has a significant advantage and also environmental protection. They used filtrate from the lower layer in alkaline condition from coal gasification fine residue was used as silicon sources to further synthesize MCM-41. They found that the remove ratio of crystal violet in water by the synthesized MCM-41 is higher than 99% with a concentration in the range of 50-400 mg/L (13). Manaa et al. investigated MCM-41 grafted with citric acid. MCM-41 was synthesized via a sol-gel method and then grafted by adding the appropriate amount of citric acid (CA). The pore sizes and volume of the CA/MCM-41 samples were found to vary markedly within CA contents. The catalytic performance of the samples was tested by the synthesis of 14-Phenyl-14H-dibenzo [a, j] xanthene (xanthene). In this reaction, the sample with 50 wt.% of CA displayed the highest acidity and catalytic activity (14). Gedikli et al. synthesized MCM-41 via hydrothermal and sonochemical synthesis methods. Their results showed that MCM-41 synthesized by the sonochemical method had higher specific surface area and pore volume than those synthesized by the hydrothermal method. Also, they investigated the effects of silica sources on the distribution of products. They found that the sodium silicate was found to be more suitable for the synthesis of MCM-41. Based on their determined optimum conditions, they also studied synthesis and characterization of MCM-41 supported Al, Co, and Fe having different ratios of metal (Metal/Si: ratio 0.05, 0.1, and 0.2). As a result, they offered to explore the catalytic properties of these catalysts (15). Laghei et al. investigated the effect of various types of post-synthetic modifications on the structure and

properties of MCM-41 mesoporous silica. They synthesized MCM-41 mesoporous silicas by hydrothermal method were subsequently modified by 3-aminopropyltrimetoxysilane (APTMS) and trimethylchlorosilane (TMCS) via two different grafting methods, i.e. attaching functional groups with or without solvent. The results confirmed that the spherical MCM-41 particles were successfully functionalized by APTMS and TMCS. Moreover, the surface area and average pore diameters of the particles were affected by the inherent properties of organosilanes such as their side chains and catalytic behaviors. The grafting methods had a tremendous impact on the obtained treated particles (16).

Among many studies, only a few studies (8) explored the differences between untreated and calcined MCM-41 samples. Therefore, this study will contribute to the literature with the help of providing more details about the calcination effect on MCM-41. In this study, MCM-41 materials were obtained via adapted sol-gel method and characterized by N₂ adsorption-desorption, Fourier transformed infrared spectroscopy (FT-IR) and scanning electron microscopy (SEM). The influence of the calcination process on the properties are discussed in detail in the discussion section.

MATERIAL AND METHOD

Sample Preparation

MCM-41 material was attained by a modified sol-gel procedure given by Martin et al. (12). Analytical grade reagents including Cetyltrimethylammonium bromide (CTAB-Alfa Aesar, 98%) by means of structure directing agent, tetraethyl orthosilicate (TEOS-Acros, 98%) by way of silica source were utilized as received. In addition, absolute ethanol (Tekkim, >99.5%), hydrochloric acid (VWR, 37%), and ammonia (Carlo Erba, 25%) were the other reagents used. According to the procedure, 40 mL of distilled water, 6 mL of ammonia, 2 g of CTAB, 60 mL of ethanol and 4 mL of TEOS were mixed using strong magnetic stirring at 30 °C for 2 h. Afterwards, a white precipitate was obtained by filtration and washed thoroughly with distilled water (12). The material obtained was divided into two parts. While half of the sample was not subjected to calcination procedure (labelled as untreated sample), the other half was calcined at 550 °C for during 6 hours in air atmosphere in a muffle furnace with 5 °C/min to eliminate the CTAB from the sample.

Characterization

The textural properties of the MCM-41s were obtained from N₂ adsorption/desorption isotherms using Micromeritics ASAP 2020 equipment. While specific surface areas were considered with respect to the Brunauer-Emmett-Teller (BET) method, the

pore size distributions were achieved using the Barret–Joyner–Hallenda (BJH) method from the N₂ adsorption/desorption isotherms. The structure was examined by SEM analysis on a Zeiss Supra VP 40 using SE2 detector at 15 kV. FT-IR spectra were logged using the Cary 630 FTIR spectrometer using the ATR technique (with a diamond-protected Attenuated Total Reflectance crystal unit) with a resolution of 4 cm⁻¹ after 100 scans in the 4000–500 cm⁻¹ wavelength range.

RESULTS AND DISCUSSION

The effect of calcination process on MCM-41 mesoporous materials are investigated in this study. Therefore, the characteristics of calcined and untreated MCM-41 were examined in detail in this section.

The surface area analysis is given in Table 1. The surface area of the untreated MCM-41 was

measured as 548.17 m²/g which is very low in proportion to the calcined one (1245.24 m²/g). This situation can be explained as the mesopores occupied by the surfactant molecules thus dropping the specific surface area. While the total pore volume of untreated MCM-41 was measured as 0.18 cm³/g, the total pore volume of calcined MCM-41 was 0.48 cm³/g. The pore diameter values of the both samples were quite similar.

The surface area of the untreated MCM-41 was quite improved when compare to the other studies in the literature (15, 18-20). Due to high surface, calcined MCM-41 material can be evaluated as promising catalyst candidate for the various applications like photocatalytic applications, adsorption, pyrolysis of the biomass, etc. Therefore, the catalytic properties of the material are worth to investigate.

Table 1: Surface area analysis of the MCM-41s.

MCM-41	Surface area (m ² /g)	Pore volume (cm ³ /g)	Average pore diameter (Å)
Untreated	548.17	0.18	18.15
Calcined	1245.2	0.48	19.00

The N₂ adsorption/desorption isotherms of the materials are given in Figure 1. Both MCM-41 samples showed similar tendencies. Depending on the IUPAC classification, type IV classification is appropriate for the mesoporous nature of the materials and reliable with previous studies. Besides, a H1-type hysteresis loop which was the appearance of mesoporous silicas was observed.

The adsorption/desorption isotherms altered slowly at a lower P/P⁰ stage, where nitrogen molecules shielded the mesoporous walls with monolayer adsorption. Besides, these isotherms showed a sharp inflection at P/P⁰ = 0.15–0.35, which confirmed that capillary condensation arose in uniform mesopores. This can be related to the N₂ molecules shielded the mesoporous walls with monolayer and multilayer adsorption. As a result,

adsorption/desorption isotherms results pointed out the presence of mesoporous structure (21).

The calcination process is known to affect the morphologies of the materials. Figure 2 displays SEM micrographs of the MCM-41s before and after the calcination process. There is no significant difference in MCM-41 framework with spherical particles with similar particle diameters. It is noticeable that most particles were almost perfectly spherical although some agglomerates were visible after calcination. This tendency could be associated with the fact that the interaction of minor particles resulted in their aggregation into numerous spherical particles with greater sizes. Besides, a huge amount of mesopores formed after the aggregation of primary units or crystallites (4).

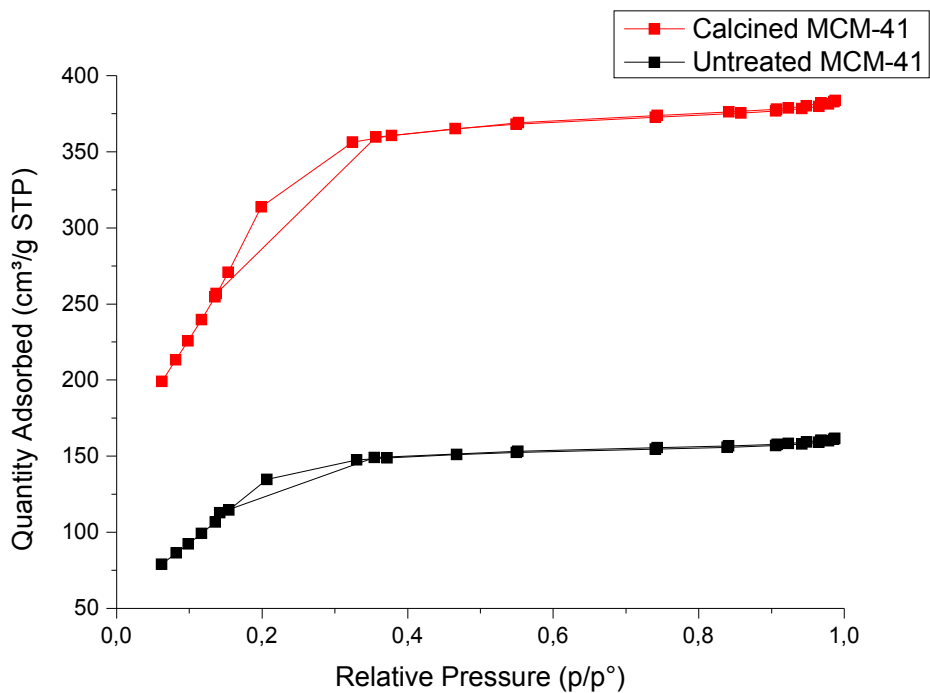


Figure 1: Nitrogen isotherms of the MCM-41s.

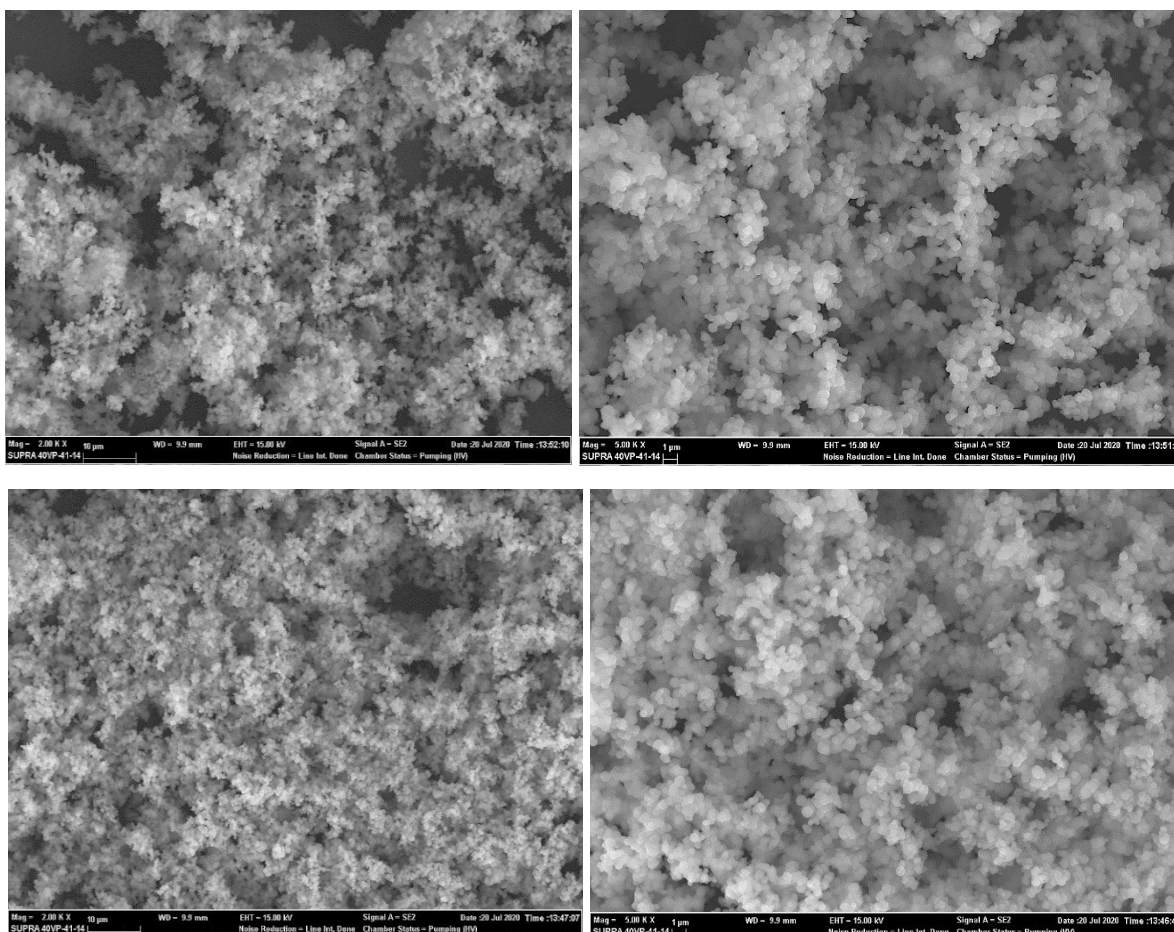


Figure 2: SEM micrographs of untreated MCM-41 (a) 2000 zoom, (b) 5000 zoom, and calcined MCM-41 (c) 2000 zoom, (d) 5000 zoom.

The FT-IR spectra are utilized to control the frequency variation in the functionality on the surfaces. FT-IR results of the MCM-41s is shown in Figure 3. It is believed that the existence of absorption bands around 2927 and 2852 cm^{-1} for the untreated sample corresponded to asymmetric and symmetric CH_2 vibrations of the organic surfactant molecules (22). The peak at 1650 cm^{-1} responded to the surface-adsorbed hydroxyl groups (4). According to Wang et al., the existence of the hydroxyl groups on the surface serves to improve of catalytic activity in such applications like photocatalytic systems due to their interacting ability with photogenerated holes to result in improved charge transfer and prevent the recombination of electron-hole pairs (4). The characteristic band for ammonium ions could be realized at 1405.57-1529.90 cm^{-1} (23). FT-IR spectra of the both materials showed the typical characteristic peaks of silica at ~ 1045 -790 cm^{-1} , agreeing to the vibrations of the Si-O-Si symmetric bond, Si-OH stretching bond and Si-O-Si asymmetric bond (23, 24). The O-H out of plane bending peak was detected at 564 cm^{-1} for only untreated MCM-41 (25).

Any band at 3500 cm^{-1} related to O-H stretching of surface hydroxyl groups indicating hydroxyl groups

and water molecules adsorbed was not detected. Besides, surface-adsorbed hydroxyl groups decreased indistinctly after calcination. In the calcined MCM-41 spectrum, the absorption peaks of 2924 cm^{-1} , 2848 cm^{-1} , and 1477 cm^{-1} existing in the untreated MCM-41 sample were vanished, signifying that CTAB was eliminated (24).

CONCLUSION

The objective of this study was to evaluate the calcination process influence on the structural properties of MCM-41. Therefore, the study dealt with the characteristic differences between untreated and calcined MCM-41 samples in terms of N_2 adsorption-desorption, FT-IR, and SEM techniques. The results demonstrate that the calcination process displays a noticeable impact on the structures. The surface area was especially improved with the calcination process. It is especially significant to highlight that some of the absorption peaks that existed in the untreated MCM-41 sample disappeared after calcination, thus signifying that the surfactants were eliminated. Further studies of the modification of the MCM-41 prepared according to this study with different metal species and catalytic applications of these materials are underway.

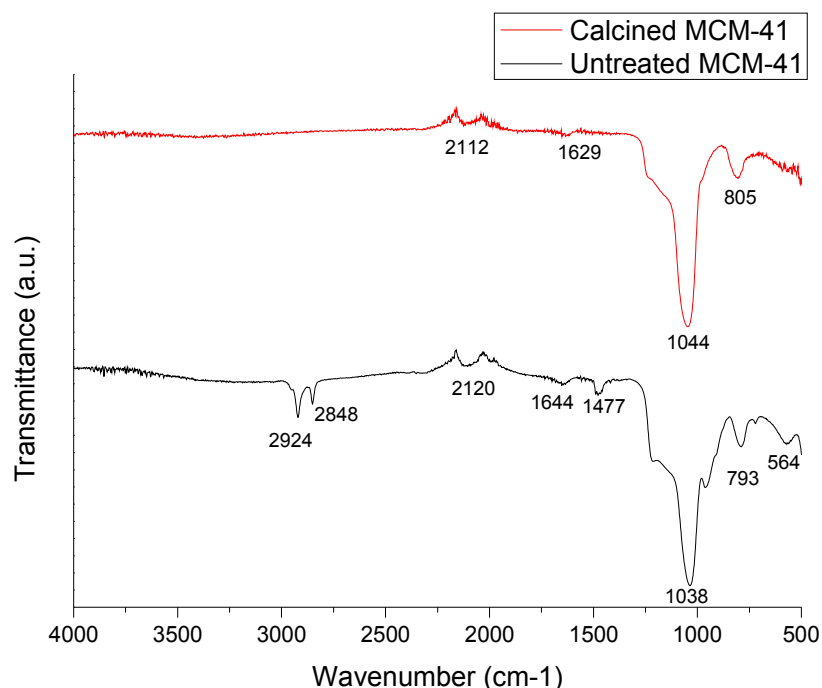


Figure 3: FT-IR spectra of the MCM-41s.

FUNDING

This study did not receive any specific grant from funding agencies in the public, commercial, or not-for-profit sectors.

REFERENCES

1. Logar N, Kaučič V. Nanoporous materials: From catalysis and hydrogen storage to wastewater treatment. *Acta Chim Slov.* 2006;53(2):117–35.

2. Dhal JP, Dash T, Hota G. Iron oxide impregnated mesoporous MCM-41: synthesis, characterization and adsorption studies. *J Porous Mater.* 2020;27(1):205-16. DOI: <https://doi.org/10.1007/s10934-019-00803-0>.
3. Galacho C, Carrott M, Carrott P. Effect of calcination parameters on structural properties of Ti-MCM-41 materials synthesized at room temperature. In: *Actas do XX Encontro Nacional da Sociedade Portuguesa de Química Campus da Caparica* [Internet]. 2006. p. 209. Available from: <https://dspace.uevora.pt/rdpc/handle/10174/6338>.
4. Wang G, Xu L, Zhang J, Yin T, Han D. Enhanced Photocatalytic Activity of Powders (P25) via Calcination Treatment. *International Journal of Photoenergy.* 2012;2012:1-9. DOI: <https://doi.org/10.1155/2012/265760>.
5. García-Labiano F, Abad A, de Diego LF, Gayán P, Adánez J. Calcination of calcium-based sorbents at pressure in a broad range of CO₂ concentrations. *Chemical Engineering Science.* 2002;57(13):2381-93. DOI: [https://doi.org/10.1016/S0009-2509\(02\)00137-9](https://doi.org/10.1016/S0009-2509(02)00137-9).
6. Lourenço JP, Fernandes A, Henriques C, Ribeiro MF. Al-containing MCM-41 type materials prepared by different synthesis methods: Hydrothermal stability and catalytic properties. *Microporous and Mesoporous Materials.* 2006;94(1-3):56-65. DOI: <https://doi.org/10.1016/j.micromeso.2006.03.020>.
7. Sohrabnezhad Sh, Jafarzadeh A, Pourahmad A. Synthesis and characterization of MCM-41 ropes. *Materials Letters.* 2018;212:16-9. DOI: <https://doi.org/10.1016/j.matlet.2017.10.059>.
8. Laghaei M, Sadeghi M, Ghalei B, Dinari M. The effect of various types of post-synthetic modifications on the structure and properties of MCM-41 mesoporous silica. *Progress in Organic Coatings.* 2016;90:163-70. DOI: <https://doi.org/10.1016/j.porgcoat.2015.10.007>.
9. He N, Lu Z, Yuan C, Hong J, Yang C, Bao S, et al. Effect of trivalent elements on the thermal and hydrothermal stability of MCM-41 mesoporous molecular materials. *Supramolecular Science.* 1998;5(5-6):553-8. DOI: [https://doi.org/10.1016/S0968-5677\(98\)00073-X](https://doi.org/10.1016/S0968-5677(98)00073-X).
10. Fellenz NA, Bengoa JF, Marchetti SG, Gervasini A. Influence of the Brønsted and Lewis acid sites on the catalytic activity and selectivity of Fe/MCM-41 system. *Applied Catalysis A: General.* 2012;435-436:187-96. DOI: <https://doi.org/10.1016/j.apcata.2012.06.003>.
11. Yin A, Wen C, Dai W-L, Fan K. Ag/MCM-41 as a highly efficient mesostructured catalyst for the chemoselective synthesis of methyl glycolate and ethylene glycol. *Applied Catalysis B: Environmental.* 2011;108-109:90-9. DOI: <https://doi.org/10.1016/j.apcatb.2011.08.013>.
12. Martin P, Rafti M, Marchetti S, Fellenz N. MCM-41-based composite with enhanced stability for Cr(VI) removal from aqueous media. *Solid State Sciences.* 2020;106:106300. DOI: <https://doi.org/10.1016/j.solidstatesciences.2020.106300>.
13. Chen H, Fu S, Fu L, Yang H, Chen D. Simple Synthesis and Characterization of Hexagonal and Ordered Al-MCM-41 from Natural Perlite. *Minerals.* 2019;30;9(5):264. DOI: <https://doi.org/10.3390/min9050264>.
14. Boukoussa B, Hamacha R, Morsli A, Bengueddach A. Adsorption of yellow dye on calcined or uncalcined Al-MCM-41 mesoporous materials. *Arabian Journal of Chemistry.* 2017;10:S2160-9. DOI: <https://doi.org/10.1016/j.arabjc.2013.07.049>.
15. Mangrulkar PA, Kamble SP, Meshram J, Rayalu SS. Adsorption of phenol and o-chlorophenol by mesoporous MCM-41. *Journal of Hazardous Materials.* 2008;160(2-3):414-21. DOI: <https://doi.org/10.1016/j.jhazmat.2008.03.013>.
16. Lu D, Xu S, Qiu W, Sun Y, Liu X, Yang J, et al. Adsorption and desorption behaviors of antibiotic ciprofloxacin on functionalized spherical MCM-41 for water treatment. *Journal of Cleaner Production.* 2020;264:121644. DOI: <https://doi.org/10.1016/j.jclepro.2020.121644>.
17. Kunchakara S, Ratan A, Dutt M, Shah J, Kotnala RK, Singh V. Impedimetric humidity sensing studies of Ag doped MCM-41 mesoporous silica coated on silver sputtered interdigitated electrodes. *Journal of Physics and Chemistry of Solids.* 2020;145:109531. DOI: <https://doi.org/10.1016/j.jpcs.2020.109531>.
18. Martínez-Edo G, Balmori A, Pontón I, Martí del Río A, Sánchez-García D. Functionalized Ordered Mesoporous Silicas (MCM-41): Synthesis and Applications in Catalysis. *Catalysts.* 2018;8(12):617. DOI: <https://doi.org/10.3390/catal8120617>.
19. Wu Y-H, Ma Y-L, Sun Y, Xue K, Ma Q-L, Ma T, et al. Graded synthesis of highly ordered MCM-41 and carbon/zeolite composite from coal gasification fine residue for crystal violet removal. *Journal of Cleaner Production.* 2020;277:123186. DOI: <https://doi.org/10.1016/j.jclepro.2020.123186>.

20. A. Mannaa M, Altass HM, Salama RS. MCM-41 grafted with citric acid: The role of carboxylic groups in enhancing the synthesis of xanthenes and removal of heavy metal ions. *Environmental Nanotechnology, Monitoring & Management*. 2021;15:100410. DOI: <https://doi.org/10.1016/j.enmm.2020.100410>.
21. Gedikli Ü, Mısırlıoğlu Z, Acar Bozkurt P, Canel AM. SYNTHESIS AND CHARACTERIZATION OF MCM-41 AND METAL-SUPPORTED MCM-41 MATERIALS USING DIFFERENT METHODS. *Commun Fac Sci Univ Ankara Ser B: Chem Chem Eng*. 2020;62(2):23–39.
22. Laghaei M, Sadeghi M, Ghalei B, Dinari M. The effect of various types of post-synthetic modifications on the structure and properties of MCM-41 mesoporous silica. *Progress in Organic Coatings*. 2016;90:163–70. DOI: <https://doi.org/10.1016/j.porgcoat.2015.10.007>.
23. Hui KS, Chao CYH. Synthesis of MCM-41 from coal fly ash by a green approach: Influence of synthesis pH. *Journal of Hazardous Materials*. 2006;137(2):1135–48. DOI: <https://doi.org/10.1016/j.jhazmat.2006.03.050>.
24. Lensveld DJ, Gerbrand Mesu J, Jos van Dillen A, de Jong KP. Synthesis and characterisation of MCM-41 supported nickel oxide catalysts. *Microporous and Mesoporous Materials*. 2001;44–45:401–7. DOI: [https://doi.org/10.1016/S1387-1811\(01\)00214-1](https://doi.org/10.1016/S1387-1811(01)00214-1).
25. Li Q, Brown SE, Broadbelt LJ, Zheng J-G, Wu NQ. Synthesis and characterization of MCM-41-supported Ba₂SiO₄ base catalyst. *Microporous and Mesoporous Materials*. 2003;59(2–3):105–11. DOI: [https://doi.org/10.1016/S1387-1811\(03\)00290-7](https://doi.org/10.1016/S1387-1811(03)00290-7).



Equilibrium and Kinetic of Ultrasound-Assisted Adsorption of Chromium (VI) ion from Electroplating Wastewater Using Melon Seed Husk Activated carbon

Esther BERNARD¹  and Adulfatai JIMOH¹ 

Department of Chemical Engineering, School of Infrastructure, Process and Engineering Technology Federal University of Technology Minna, PMB 65, Niger State, Nigeria.

Abstract: This study was focused on the removal of Cr(VI) ions from electroplating wastewater by ultrasound-assisted adsorption onto activated carbon obtained from melon seed husk. The activated carbon was produced by carbonization of crushed melon seed husk at a temperature of 500 °C for 15 min and further activation using 1.0 M concentration of potassium chloride (KCl) at a temperature of 500 °C for 90 min in a muffle furnace. The obtained adsorption isotherm data were better fitted to the Langmuir model than Freundlich model for adsorption both in the presence and absence of ultrasound (US). The adsorbent maximum adsorption capacity for Cr(VI) ion obtained from the Langmuir isotherms, were 5.059 mg/g and 2.031 mg/g both in the presence of ultrasound and its absence, respectively. The adsorption process in the presence and absence of ultrasound obeyed the pseudo-second-order kinetics. The SEM image of activated carbon before adsorption of metal ion revealed that the surface of activated carbon contains pores with different sizes and shapes, and also showed a significant change on the surface of activated carbon after interaction with Cr(VI) ions.

Keywords: Carbonization, activated carbon, melon seed husk, ultrasound-assisted adsorption.

Submitted: November 03, 2020. **Accepted:** November 11, 2021.

Cite this: Bernard E, Jimoh A. Equilibrium and Kinetic of Ultrasound-Assisted Adsorption of Chromium (VI) ion from Electroplating Wastewater Using Melon Seed Husk Activated carbon. JOTCSB. 2021;4(2):35-46.

***Corresponding author. E-mail:** estherbernard667@gmail.com.

INTRODUCTION

Currently, water contamination is a worldwide issue, with heavy metals contamination causing one of the most significant problems (1). Heavy metals are non-degradable, they are persistent, and accumulative in nature; hence they are carcinogenic agents that cause a serious threat to the living population (2). Nonetheless, certain heavy metals in little amounts are fundamental for a healthy life, yet enormous amounts and prolonged contact with these heavy metals may cause chronic toxicity. The toxicity caused by heavy metals includes reduced mental and central nervous function, gastrointestinal disorders, paralysis, ataxia, stomatitis, lowered energy level, damaging of the liver, lungs and other essential organs (3). Heavy metals are present practically in every region of present-day commercialization, from medicines to processed foods, construction materials to

cosmetics; appliances to personal care products. It is very hard to avoid exposure to any of the many harmful heavy metals that are widespread in our environment (3). Among these metals, lead, nickel, cadmium, platinum, copper, lead, chromium, mercury, arsenic and antimony are of foremost concern (4). The effective recapture of heavy metals from wastewater and industrial wastewater before being disposed into the environment is of exceptional concern to researchers and engineers because of their unsafe impacts on humans and numerous living things. Thus, primary importance has been devoted to the need for the treatment of industrial wastewater effluent and as such both local and international authorities have established policies that made it mandatory for industrial wastewater to be treated to meet a set standard before being discharged into aqueous bodies (Table 1). To achieve such set standards, numerous methods have been employed for the treatment of

water contaminated with heavy metals. These methods include membrane processes, chemical precipitation, solvent extraction, electrochemical reduction, ion exchange, lime softening, coagulation/flocculation, and chitosan graphene oxide nanocomposites. Nevertheless, most of these mention treatment methods have limitations which include bulk poisonous sludge generation in flocculation/coagulation methods, renewal

requirements during ion exchange, high operation cost, and large amounts of chemicals required using the chemical precipitation method (4).

However, the search for new methods that are sustainable in terms of efficiency, economy, energy, and environmentally friendly for the treatments of heavy metals in wastewater has attracted attention to the adsorption techniques (5).

Table 1: Permissible limits of heavy metals in drinking and wastewater by international institutes.

Heavy metals	Permitted limits WHO*/EPA** (mg L ⁻¹)	References
Zinc	5	(4)
Copper	1.0-1.5	(6)
Lead	0.005-0.015	(7)
Chromium	0.05-0.25	(4)
Arsenic	0.01	(4)
Mercury	0.002	(4)
Cadmium	0.005	(4)
Beryllium	0.004	(4)
Nickel	0.1	(7)

The use of activated carbon (AC) employed as adsorbent for the adsorption process has gained enormous attention due to its high internal surface area, small particle sizes, and active free valences. However, it might not be employed as an adsorbent for large-scale water treatment as a result of its high cost of production (4).

In recent times, low-cost and abundantly available natural materials such as agricultural waste materials have been employed as adsorbents and used to produce activated carbon for the removal of heavy metals in wastewater. These studies include rice husk, coir pith, orange peel, sawdust, peat, soybean, pine bark, banana peel and pith, rice bran cottonseed hulls, hazelnut shells, wool fibers, coconut shell, and saffron corn (8). Previous research has also shown that melon seed husk (*Citrullus colocynthis* L) is readily available and a good adsorbent for the removal of heavy metals. Melon belongs to the class of cucurbitaceae family, they are well-known to contain high oil and protein contents. It contains up to 35 % protein and 50 % oil, which is responsible for its wide cultivation and consumption worldwide (9). Melon seed husk has been used from adsorption studies of malachite green (10), Ni(II), Cr(III) and Co(II) (11) as well as Pb(II) and Cd(II) (12).

Although activated carbon has proven to be a suitable adsorbent, however, the relatively low adsorption rate of activated carbon due to its microporous and long diffusion pathway has necessitated the need for possible enhancement

using ultrasonic irradiation. Ultrasound irradiation has been confirmed to accelerate the mass transfer process as a result of the phenomenon known as acoustic cavitation (13). Cavitation is the formation, growth, and consequent collapse of bubbles over a short time frame resulting in the generation of large degrees of energy over a specific location. Acoustic cavitation is the sound wave between the range of 16-100 kHz that produce pressure vibrations to generate the essential cavitation intensity (14). The employment of ultrasonic cavitation technology for wastewater treatment has been reported by researchers, although not yet been fully exploited (14). Raya and Zaria reported the use of rice husk activated carbon irradiated with ultrasound for the removal of Pb(II) in aqueous wastewater. The irradiated activated carbon adsorption capacity improved to 16.67 mg/g as against 9.80 mg/g when there was no irradiation and the process was described by the Langmuir isotherm model. Their findings showed that activated carbon adsorption capacity irradiated with ultrasonic waves was almost twice as much as the capacity of activated carbon adsorption without irradiation (15). Entezari and Soltani, reported the use of saffron corm irradiated with ultrasound for removal of Pb(II) and Cu(II) from binary aqueous solution, the obtained result indicates that the removal of both metal ions was greater in the presence of ultrasound than in absence of ultrasound (16). Furthermore, Schueller and Yang in their work found out that ultrasound acted as a mixer, which improved the mass transfer coefficients by means of cavitation and acoustic streaming (16). Since adsorption process is an easy

technique for the removal of pollutants from water and wastewater and the use of a cheaply available adsorbent which poses a high capacity for the removal of pollutants is very essential. Likewise, since the diffusion of species has a significant role in the adsorption process. Thus, the blending of the two referenced points was considered in this investigation. Activated carbon produced from melon seed husks was used as an adsorbent for the removal of Cr(VI) from electroplating wastewater in the presence and absence of ultrasound.

The main purpose of this study is the use of ultrasound to aid adsorption of Cr(VI) ions from industrial wastewater (electroplating wastewater) onto activated carbon prepared from melon seed husks. The cavitation effects generated during ultrasonication, creates shear stress that break up the activated surface and permits penetration of metal ions into the pores, also a localized turbulence of the solid-liquid film, during ultra-sonication

accelerates the rate of mass transfer through the film by increasing the intrinsic mass transfer coefficient further pushes the adsorbates into the micropores. This increases pore division coefficient and increase the rate of adsorption.

Several research works has been carried out in the past, using activated carbon derived from agricultural waste products as adsorbent for the removal of different metal ions from simulated wastewater (aqueous wastewater) in absence of ultrasound. Although few works have been carried out on adsorption of metal ions from aqueous wastewater in presence of ultrasound (aided by ultrasound), none has been carried out with industrial wastewater (electroplating wastewater) in the presence of ultrasound. Table 2 shows previous works of the adsorption capacities (calculated from the Langmuir isotherm model) of activated carbon (obtained from agricultural waste products) of metal ions from aqueous wastewater.

Table 2: Activated carbon from Agricultural waste.

Agricultural waste	Adsorptive	Q _m (mg/g)	Reference
Cob of the corn	Cu(II)	5.84–7.89	(17)
Melon seed husk	Ni(II)	-12.75	(11)
Melon seed husk	Co(II)	-38.39	(11)
Activated Carbon from Rice Husk,	Pb(II)	16.67 ^a	(17)
		9.80 ^b	
Hazelnut shell activate carbon	Cu(II)	3.05 ^a	(17)
		3.77 ^b	
Cob of the corn	Mn(VI)	0.53	(18)
Maple sawdust	Cd(II)	3.19	(19)
Bamboo-based Activated Charcoal	Pb(II)	4.792	(19)
Bamboo-based Activated Charcoal	Cd(II)	4.594	(19)
Bamboo dust	Pb(II)	4.771	(19)
Bamboo dust	Cd(II)	4.400	(19)

^a in the presence of US

^b in the absence of US

MATERIALS AND METHODS

Materials

Melon seed husk sample was obtained from Mina, Niger State, Nigeria. The husk was washed thoroughly with distilled water to remove foreign materials present on the surface. The washed sample was further oven-dried at a temperature of 100 °C and crushed with a mechanical crusher to reduce the size. The crushed samples were carbonized at a temperature of 500 °C for 15 min. 25 g of the carbonized sample was mixed in 50 mL of 1.0 M concentration of potassium chloride and allowed to soak for 24 h at room temperature. It was later oven-dried for 30 min at 100 °C. The dried carbonized samples were further transferred into a muffle furnace and activated at a temperature of 500 °C for 90 min. The obtained activated carbon was then transferred into a desiccator to cool. Thereafter the sample was carefully rinsed using 0.1

M of HCl and distilled water to eliminate the residual salt present until the pH of filtrate reached 7.

Batch Adsorption Experiment

Set-up

Adsorption study was carried out using an ultrasonic cleaning bath, with model number SB25-12DT, operating at 40 kHz and equipped with a temperature regulator. Distilled water was added to the cleaning bath up to one third (1/3) of the volume of the cleaning bath. 0.6 g of activated carbon was added into 50 mL of electroplating wastewater of known concentration and pH which was kept in 250 mL Erlenmeyer flasks, which were placed into the carrier fitted in the ultrasonic bath. A temperature of 30 °C was maintained during ultrasonic irradiation by water circulating from a thermostatic bath utilizing a pump. The suspensions were sonicated for a given period time and the operating frequency was maintained at 40 kHz.

Adsorption studies were also carried out in the absence of ultrasound (conventional method) using a water-bath shaker with an operating speed of 200 rpm and at 30 °C.

Equilibrium experiments

The industrial wastewater used was collected from the electroplating section of the Scientific Equipment Development Institute (SEDI), Niger State. The wastewater contained Cr(VI) ions. The initial concentration of Cr(VI) found in the wastewater sample was 18.28 ppm. The initial pH of the wastewater was 3.5 and was adjusted to pH 4 for adsorption studies using 0.1 N NaOH.

The equilibrium adsorption experiment was conducted in 250 mL Erlenmeyer flasks containing 0.6 g of adsorbent with 50 mL of electroplating wastewater which was sonicated for 90 min in an ultrasonic cleaning bath until equilibrium was reached. Adsorption studies using the conventional method were also carried out in 250 mL Erlenmeyer flasks containing 0.6 g of adsorbent with 50 mL of electroplating wastewater. The flasks were agitated for 90 min at 200 rpm. After the sonication and agitation, the supernatant was centrifuged and analyzed using an atomic absorption spectrophotometer for residual metal ions concentration.

The amount of Cr(VI) ions adsorbed at any given time was calculated using equation (1).

$$q = \frac{(C_0 - C)V}{M} \quad (1)$$

Where q is the number of metal ions (Cr(VI) ions) adsorbed at time t, C₀ and C are the initial metal ions concentrations and metal ions concentrations at time t respectively. V is the volume of wastewater used (50 mL) and M is the amount of adsorbent in industrial wastewater (0.6 g) used.

RESULTS AND DISCUSSION

Characterization of Activated Carbon

The prepared activated carbon from melon seed husk by a two-step process of carbonization at 500 °C for 15 minutes and then activation with KCl at 500 °C for 90 min was characterized by standard methods (Table 3). The obtained specific surface area by BET analysis was 1285.75 m²/g and the obtained iodine number of 1251 mg/g are the highest so far reported for activated carbon obtained from the melon husk. Formaldehyde and sodium hydroxide (20) impregnated activated carbons from melon husk had a specific surface area of 395 and 1187 m²/g respectively. Therefore, the prolonged impregnation with KCl and the two-step activation process adopted favored the formation of porous activated carbon.

Table 3: The properties of activated carbon prepared from melon seed husk.

Characteristic	Method	Value
Specific surface area	BET, N ₂	1285.751 m ² /g
Iodine value	ASTM D 4607	1251 mg/g
Ash	ASTMD2866	9.0
Total Pore volume	ASTMD 4607	0.47 cm ³ /g
Pore size		3.191 cm ³ /g

Adsorption Isotherms

The adsorption of Cr(VI) from electroplating wastewater on activated carbon from the melon husk (AC) was conducted in the presence and absence of ultrasound (US) at 30 °C. As shown in Figure 1, the amount of Cr(VI) adsorbed on AC in the presence of the US is greater than the amount in absence of the US. The increased amount of adsorbed Cr(VI) on AC in presence of the US is a result of acoustic cavitation which is the formation, growth, and violent collapse of cavitation bubbles. Also, the shear forces generated during the cavitation are typically mostly responsible for the enhanced removal of the metal ions in the presence of the US (17).

To investigate and further describe adsorption, isotherm models were employed. The most frequent models used are the Langmuir and Freundlich isotherms (Table 4). In this current work, the

relationships between the amount of Cr(VI) adsorbed and its equilibrium concentration in wastewater in the presence and absence of US for 90 min at 30 °C were modeled by both Langmuir and Freundlich isotherm models. The Langmuir model is used to describe the homogeneous sorption, in which each sorption molecule has equal sorption energy as the other, while the Freundlich isotherm is used to describe sorption characteristics for the heterogeneous surface. Langmuir constants a_L and q_m and Freundlich constants K_F and b_F are presented in Table 5. The ratio of adsorption and desorption is defined by Langmuir adsorption constant a_L and it is also related to the free energy of adsorption.

Figures 2 and 3 showed that the two isotherms models employed both in the presence of the US and in its absence were well fitted by both models used as a result of the good fits attained (R² close to

1). However better fitting was provided by the Langmuir model.

The value of a_L represents the affinity of Cr(VI) to the adsorbent. The value of a_L for US-adsorption was higher when compared to adsorption in absence of US as evident in Table 5, which implies that the introduction of US positively affected the affinity of

Cr(VI) on AC. Identical findings were obtained by Milenković *et al.* (8) for the adsorption of Cu(II) ions on hazelnut activated carbon in the presence of US at a frequency of 40 kHz. A similar observation was drawn from values of Freundlich constant K_F , which has a higher value in the presence of the US than its value in the absence of US adsorption.

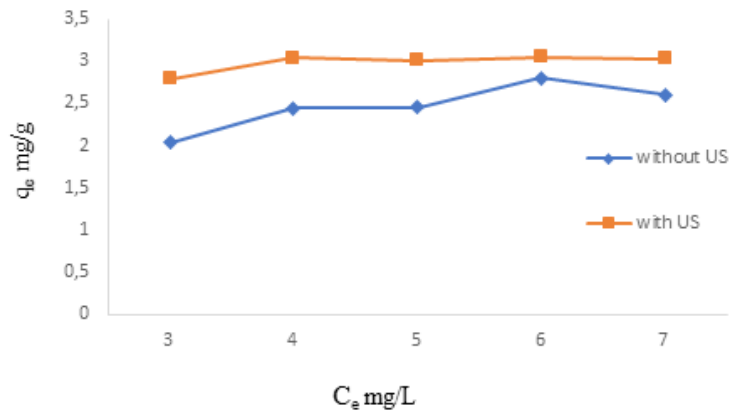


Figure 1: Adsorption isotherms of Cr(VI) ions on AC from melon seed husks in the absence (◆) and the presence (■) of ultrasound at 30 °C.

Table 4: Adsorption isotherms.

Isotherm	Integral form	Linear form
Langmuir	$q_e = \frac{k_L C_e}{1 + a_L C_e}$	$\frac{C_e}{q_e} = \frac{1}{k_L} + \frac{a_L}{k_L} \times C_e$
Freundlich	$q_e = K_F C_e^{b_F}$	$\ln q_e = \ln K_F + b_F \ln C_e$

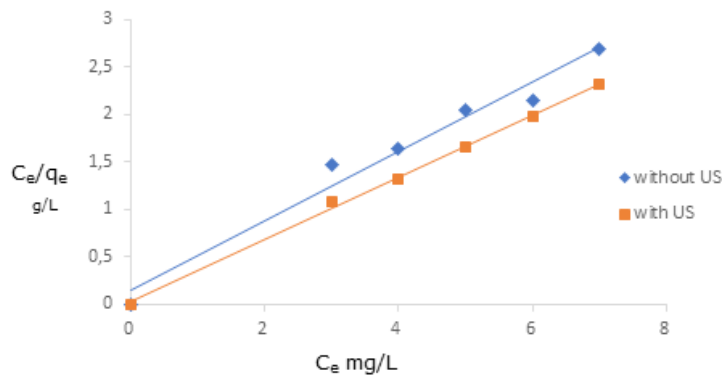


Figure 2: Linear forms of the Langmuir model adsorption isotherms of Cr(VI) ions on AC from melon seed husks in the absence (◆) and the presence (■) of ultrasound at 30 °C.

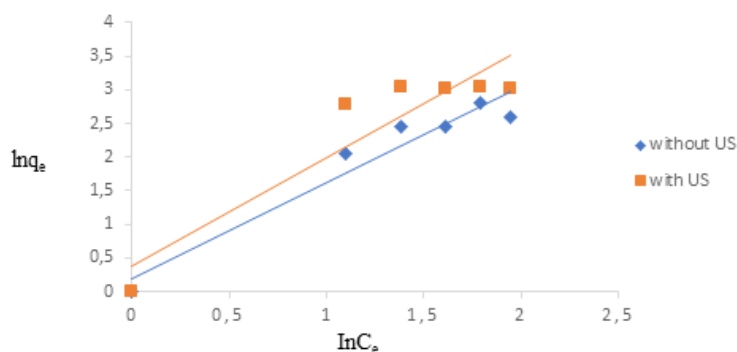


Figure 3: Linear forms of the Freundlich adsorption isotherms of Cr(VI) ions on AC from melon seed husks in the absence (♦) and the presence (■) of ultrasound at 30 °C.

Table 5: Adsorption isotherms parameters, linear correlation coefficient, and standard deviation.

Isotherm	Parameter	Silent adsorption	Ultrasound-assisted adsorption
Langmuir	a _L (L/mg)	2.591	11.802
	q _m (mg/g)	2.031	5.059
	R	0.998	0.972
Freundlich	b _F	1.425	1.606
	K _F	1.218	1.474
	R	0.939	0.863

It was also observed from Table 5 that the monolayer saturation capacity at equilibrium q_m in the presence of US was larger than that in the absence of US adsorption (2.031 mg/g and 5.059 mg/g respectively), which could be ascribed to cavity effects that aid the adsorption process.

Figure 4 shows the amount of Cr(VI) ions adsorbed on AC obtained from melon seed husk both in the presence of US and adsorption in the absence of US at 30 °C. The adsorption study was carried out up to a contact time of 135 min to obtain equilibrium time. At the start of the adsorption process Cr(VI) ions were swiftly adsorbed, but which later slowed down, until equilibrium was finally reached. The

highest rate of Cr(VI) ion removal at the start of adsorption was perhaps due to the available large surface area on the adsorbent existing for adsorption and the strong interaction amongst the Cr(VI) ions and the surface of the adsorbent. At the later stage of the adsorption process, the surface adsorption sites became exhausted and the rate of removal was controlled by the rate of Cr(VI) ion transportation from the external to the internal sites of the adsorbent particles. In the presence of ultrasound, the removal of Cr(VI) was higher than in the absence of ultrasound and this could be attributed to the result of the cavitation process which enhances the diffusion process.

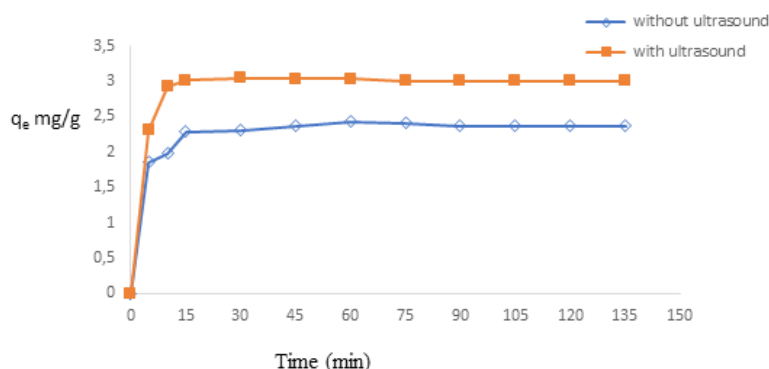


Figure 4: Adsorption of Cr(VI) ions on AC from melon seed husk in the absence (◊) and the presence (■) of ultrasound at 30 °C.

Adsorption kinetics mechanism

Three kinetic models namely the pseudo-first-order, pseudo-second-order and intraparticle diffusion were employed to study the controlling mechanism of the adsorption process of Cr(VI) ions on the adsorbent in this current study. Several steps are involved in the liquid-solid adsorption process, which includes the diffusion of the solute from the solution to the film surrounding the sorbent particles, the solute diffusion from the particle surface through the pores into the internal active sites, and the adsorption of solute from active sites by various mechanisms. The entire sorption rate is controlled by the rate of each step. The differential, integral, and linear forms of the kinetic models are shown in Table 5. The values of the kinetic model parameters used and the linear forms of the linear correlation coefficient are shown in Table 6. When the pseudo-second-order kinetics was applied, the values of equilibrium amount of Cr(VI) ions adsorbed q_e , was obtained from the non-linear regression, and considering that the exponential growth of the amount of Cr(VI) ions adsorbed with

time ($q_e = 2.999$ and 2.489 mg/g for adsorption in presence of ultrasound and absence of ultrasound respectively).

From the plot of the linear forms of the three kinetic model curves shown in Figure 5, it was observed that only the pseudo-second-order kinetic model applied fitted well with the experimental data, which has a linear correlation coefficient of 1. The pseudo-second-order kinetic model shown in Figure 6 has the best fit to the experimental data for both adsorptions in the presence of ultrasound and adsorption in the absence of ultrasound. The pseudo-second-order kinetic model assumes that rate-limiting steps could be a result of a chemical reactions between adsorbent and adsorbate. Therefore, the pseudo-second-order kinetic model is possibly the generalized kinetic model for the adsorption system studied. Milenković et al (8) reported related findings of the applicability of a similar kinetic model and the second-order nature of adsorption of Cu(II) ions on activated carbon gotten from hazelnut shells.

Table 6: Kinetic Models.

Kinetic Model	Differential form	Integral form	Linear form
Pseudo-first order	$\frac{dq}{dt} = k_1(q_e - q)$	$q = q_e(1 - e^{-k_1 t})$	$\ln\left(\frac{q_e - q}{q_e}\right) = -k_1 t$
Pseudo-second order	$\frac{dq}{dt} = k_2(q_e - q)^2$	$q = \frac{k_2 q_e^2 t}{1 + k_2 q_e t}$	$\frac{t}{q} = \frac{1}{k_2 q_e^2} + \frac{1}{q_e} t$
Intra-particle diffusion	$\frac{\partial q}{\partial t} = D_{eff} \frac{\partial^2 q}{\partial t^2}$	$q = k_p \sqrt{t} + C_1$	$q = k_p \sqrt{t} + C_1$

Table 7: Parameters of kinetic models and linear correlation coefficient deviation.

Kinetic Model	Model Parameters	Silent Adsorption	Ultrasound-assisted adsorption
Pseudo-first order	$k_1(\text{min}^{-1})$	0.009	0.004
	R	0.513	0.142
Pseudo-second order	$K_2(\text{g/mg min})$	1.178	9.756
	q_e	2.489	2.999
	R	0.999	1.000

Intraparticle diffusion			
First Stage	Kp (mg/g min ^{0.5})	0.129	0.152
	C ₁ (mg/g)	1.231	1.683
	R	0.501	0.422

In the present study, of the three kinetic models employed, the pseudo-second-order model gave the best fit of experimental data and has the highest linear correlation coefficient of R = 1 and R= 0.999 for adsorption in presence of US and absence of US respectively. The Pseudo-second-order model is founded on the assumption that the rate-limiting step may well be a chemical reaction between the adsorbent and the adsorbate. Thus, for the adsorption system studied, the possibly generalized kinetic model is the pseudo-second-order kinetic. Babarinde et al (11) reported the applicability of a

similar kinetic model and the second-order nature of the adsorption process of Cr(VI) ion on melon seed husk as adsorbent. The rate constant for the reaction of pseudo-second-order was positively affected the US in the present study, its values being K₂ = 9.756 g/mg min and K₂ = 1.178 g/mg min in the presence and absence of US, respectively. The intra- particle diffusion model was also employed to identify the diffusion mechanism because both the pseudo-first-order model and the pseudo-second-order model could not identify it.

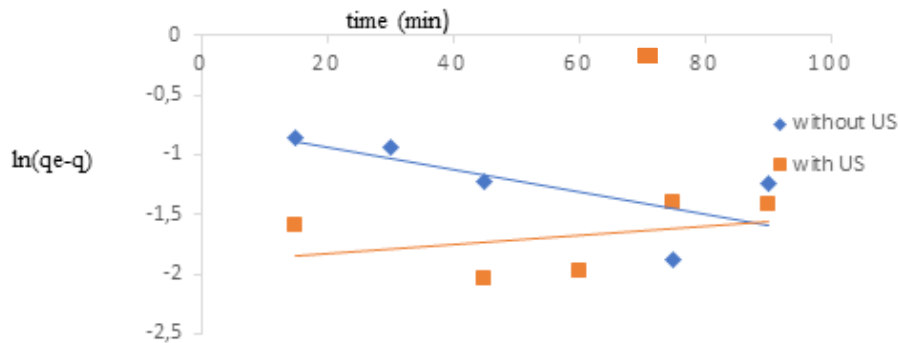


Figure 5: Pseudo-first-order kinetic model for the removal of Cr(VI) ions on AC from melon seed husk in the absence (♦) and the presence (■) of ultrasound at 30 °C.

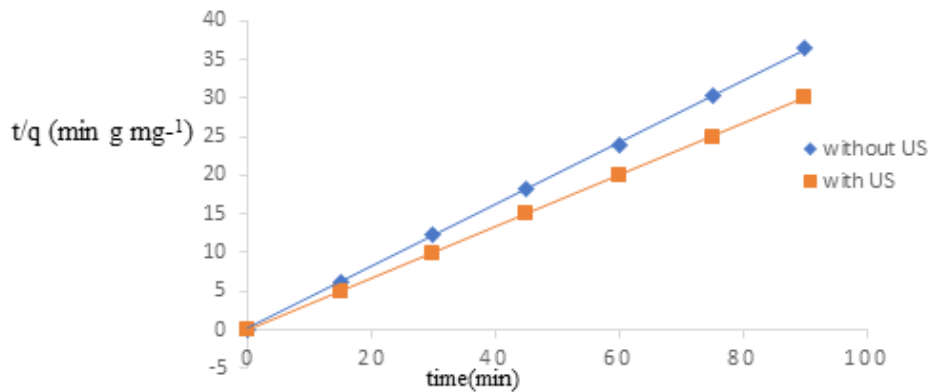


Figure 6: Pseudo-second-order kinetic model for the removal of Cr(VI) ions on AC from melon seed husk in the absence (♦) and the presence (■) of ultrasound at 30 °C.

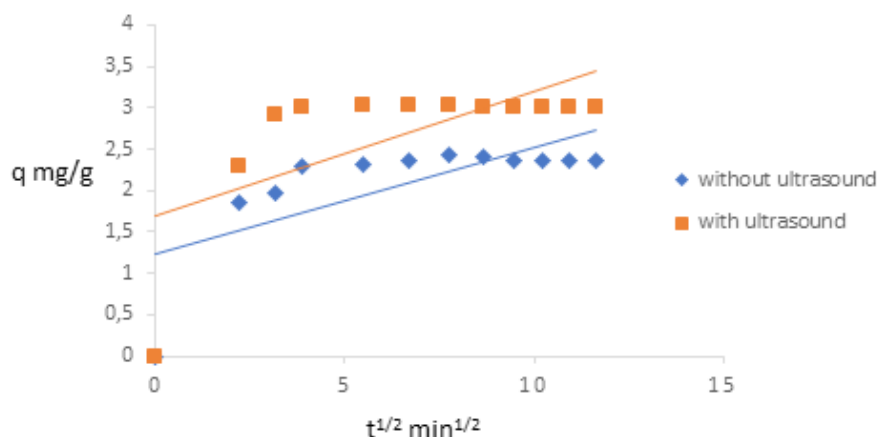


Figure 7: Intra particle diffusion model for the removal of Cr(VI) ions on AC from melon seed husk in the absence (♦) and the presence (■) of ultrasound at 30 °C.

Figure 7 shows the plot of q versus $t^{1/2}$ both in the presence and absence of US. Intraparticle diffusion is the sole rate determining step if the plot of qt versus $t^{1/2}$ is linear and passes through the origin ($C = 0$). In the adsorption process, the plot did not pass through the origin, which specifies the existence of some boundary layer effect and disclosed that intraparticle diffusion is not the rate determining step in overall sorption process.

When comparing the adsorption in absence of ultrasound (silent adsorption) to that in presence of ultrasound, the intra-particle diffusion rates in the presence of US has increased approximately by 18% compared to adsorption in absence of US. The intercept value C_1 for both adsorptions in presence

of US and absence of US is given in Table 6. The greater intercept value (C_1) in presence of the US depicts higher ultrasound-assisted adsorption of activated carbon from the melon seed husk, compared to adsorption in absence of ultrasound (21).

The SEM image of AC before adsorption of metal ions shown in Figure 8 (a), revealed that the surface of AC contains pores with different sizes and shapes, while Figure 8 (b), revealed that there were significant changes on the surface of AC after interaction with Cr(VI) ions. Some of the pores before adsorption have been closed after interaction with Cr(VI) ions and flake like deposits were also observed on the surface of AC after adsorption.

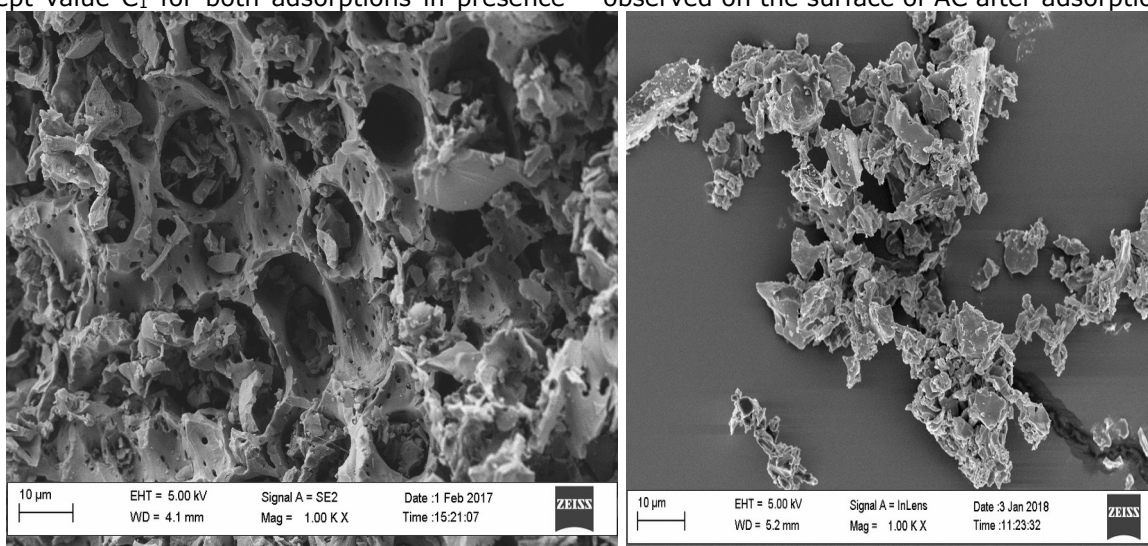


Figure 8: SEM images of AC (left) before and after (right) adsorption at 1,000 magnification.

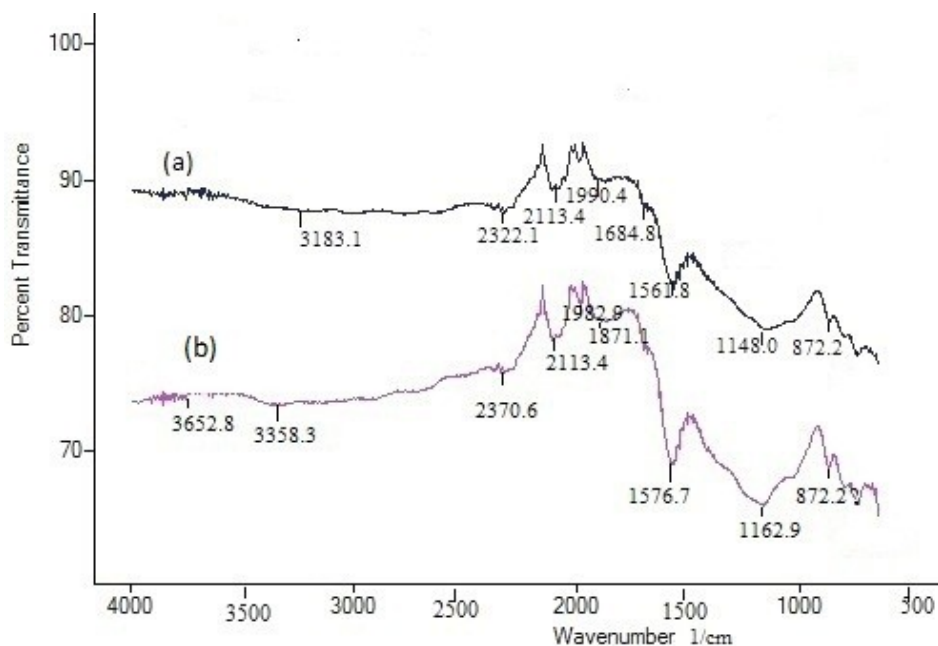


Figure 9: FTIR analysis of activated carbon from melon husk (ACM) and ACM after adsorption.

The FTIR spectrum of the activated carbon from melon husk was carried out to reveal the active surface functional groups, responsible for binding of Cr(VI) ion. The FTIR spectra (a) of activated carbon showed O-H stretching band, of decreased intensity, appeared at 3183.1 cm^{-1} , due to cleaving of phenolic groups during activation, the O-H stretching band at 3183.1 cm^{-1} present on the FTIR spectra of activated carbon (a) was shifted to 3358.3 on the FTIR spectra (b) of activated carbon loaded with Cr(VI) ions with appearance of a new band at 3652.8 cm^{-1} after adsorption. Similarly, the peaks at 2322.1 , 1561.8 and 1148.0 cm^{-1} present on the FTIR spectra (a) of activated carbon (were shifted to 2370.6 , 1576.7 and 1162.9 cm^{-1} on the FTIR spectra (b) of activated carbon respectively after adsorption, the shift in positions was as a result of attachment of the Cr(VI) ions to the activated carbon through these functional groups. While the peak at 1684.8 cm^{-1} present on the FTIR spectra (a) of activated carbon disappeared after adsorption of Cr(VI) ions as evident in spectra (b). The disappearance of peak suggest that there was chemical interactions between the adsorbed Cr(VI) ions and functional groups. The result is consistent with the works of Giwa *et al* (2013) of which the FTIR spectra of the activated carbon obtained from melon husk had a shift in the position of the functional group of C=O and -NH at 1624 cm^{-1} and 3454 cm^{-1} , were shifted to 1629 cm^{-1} and 3448 cm^{-1} respectively after adsorption of cadmium ion.

CONCLUSION

A two-step process of carbonization and subsequently chemical activation was employed for the production of activated carbon from melon seed husk with a higher specific surface area compared

to other activated carbons previously produced from melon seed husk. This implies that carbonization and subsequent chemical activation lead to activated carbon with well-developed pores. The average pore size suggested that the produced activated carbons are mainly mesoporous. The obtained adsorption isotherm data for removal of Cr(VI) ion from electroplating wastewater was well fitted to the Langmuir model than the Freundlich model for both adsorptions assisted by ultrasound and adsorption in absence of ultrasound. Higher R values were obtained from the Langmuir model, which could be possibly due to the homogeneous distribution of active sites on the activated carbon surfaces. Furthermore, the kinetics of Cr(VI) ion adsorption on the melon seed husk activated carbon follows the pseudo-second-order model, which indicates that chemisorption may be the rate-limiting step. The prime benefit of sonication based on the data obtained was a higher speed of adsorption, particularly during the initial period. In the presence of ultra-sonication, the rate constant of pseudo-second-order was increased by 88 % when compared to that in the absence of ultra-sonication. Activated carbon from melon seed husk is an effective adsorbent for removal of Cr(VI) ion from electroplating wastewater, even though the production process was relatively simple and from a cheap available waste product, the conclusion of the use of activated carbon obtained from melon seed husk for removal of Cr(VI) ion, other heavy metals and other pollutants should only be withdrawn when after only a thorough techno-economic analysis of the complete removal process. The SEM image showed a significant change after the adsorption of Cr(VI) ions.

REFERENCES

1. Alghamdi AA, Al-Odayni A-B, Saeed WS, Al-Kahtani A, Alharthi FA, Aouak T. Efficient Adsorption of Lead (II) from Aqueous Phase Solutions Using Polypyrrole-Based Activated Carbon. *Materials*. 2019 Jun 24;12(12):2020. [<DOI>](#).
2. Rao RAK, Kashifuddin M. Kinetics and isotherm studies of Cd(II) adsorption from aqueous solution utilizing seeds of bottlebrush plant (*Callistemon chisholmii*). *Appl Water Sci*. 2014 Dec;4(4):371–83. [<DOI>](#).
3. Chaturvedi D, Sahu O. Adsorption of heavy metal ions from wastewater. *Global Journal of Environmental Science and Technology*. 2014;2(3):020–8.
4. Shafiq M, Alazba A, Amin M. Removal of heavy metals from wastewater using date palm as a biosorbent: a comparative review. *Sains Malaysiana*. 2018;47(1):35–49.
5. Kanawade SM, Gaikwad R. Removal of zinc ions from industrial effluent by using cork powder as adsorbent. *International journal of chemical engineering and applications*. 2011;2(3):199.
6. Bilal M, Shah JA, Ashfaq T, Gardazi SMH, Tahir AA, Pervez A, et al. Waste biomass adsorbents for copper removal from industrial wastewater—A review. *Journal of Hazardous Materials*. 2013 Dec;263:322–33. [<DOI>](#).
7. Abdel-Raouf M, Abdul-Raheim A. Removal of heavy metals from industrial waste water by biomass-based materials: a review. *J Pollut Effects Control*. 2017;5(1):1–13.
8. Milenković DD, Dašić PV, Veljković VB. Ultrasound-assisted adsorption of copper(II) ions on hazelnut shell activated carbon. *Ultrasonics Sonochemistry*. 2009 Apr;16(4):557–63. [<DOI>](#).
9. Giwa S, Abdullah LC, Adam NM. Investigating "Egusi" (*Citrullus Colocynthis* L.) Seed Oil as Potential Biodiesel Feedstock. *Energies*. 2010 Mar 30;3(4):607–18. [<DOI>](#).
10. Idris S, Yisa J, Muhammed NM, Chioma C. Equilibrium and Adsorption Studies of Malachite Green onto Melon Seed Shell Activated Carbon. *Int J Modern Chem*. 2013;4(2):90–103.
11. Babarinde A, Omisore GO, Babalola JO. Kinetic, isothermal and thermodynamic parameters for the biosorption of Ni (II), Cr (III), and Co (II) onto Melon (*Citrillus lanatus*) seed husk. *International Journal of Chemical and Biochemical Sciences*. 2014;6:18–33.
12. Nwankwo D, Sylvanus Chima E, Tochukwu M. Comparative study of the Bioadsorption of Cadmium and lead from industrial waste water using melon (*citrullus colocynthis*) husk activated with sulphuric acid. *American Journal of Environmental Protection*. 2014;1(1):1–8.
13. Hamdaoui O, Naffrechoux E. Adsorption kinetics of 4-chlorophenol onto granular activated carbon in the presence of high frequency ultrasound. *Ultrasonics Sonochemistry*. 2009 Jan;16(1):15–22. [<DOI>](#).
14. Parthasarathy S, Mohammed RR, Fong CM, Gomes RL, Manickam S. A novel hybrid approach of activated carbon and ultrasound cavitation for the intensification of palm oil mill effluent (POME) polishing. *Journal of Cleaner Production*. 2016 Jan;112:1218–26. [<DOI>](#).
15. Raya I, Zakir M. The adsorption of Pb (II) ions on activated carbon from rice husk, irradiated by ultrasonic waves: kinetic and thermodynamics studies. *Journal of Natural Sciences Research*. 2014;4(2):18–24.
16. Entezari MH, Soltani T. Simultaneous removal of copper and lead ions from a binary solution by sono-sorption process. *Journal of Hazardous Materials*. 2008 Dec;160(1):88–93. [<DOI>](#).
17. Milenković DD, Bojić ALj, Veljković VB. Ultrasound-assisted adsorption of 4-dodecylbenzene sulfonate from aqueous solutions by corn cob activated carbon. *Ultrasonics Sonochemistry*. 2013 May;20(3):955–62. [<DOI>](#).
18. Norozi F, Haghdoost G. Application of corncob as a natural adsorbent for the removal of Mn (VII) ions from aqueous solutions. *Orient J Chem*. 2016;32(4):2263–8.
19. Odoemelam SA, Onwu FK, Uchechukwu SC, Chinedu MA. Adsorption isotherm studies of Cd (II) and Pb (II) ions from aqueous solutions by bamboo-based activated charcoal and bamboo dust. *American Chemical Science Journal*. 2015;5(3):253–69.
20. Foo KY, Hameed BH. Preparation and characterization of activated carbon from melon (*Citrullus vulgaris*) seed hull by microwave-induced NaOH activation. *Desalination and Water Treatment*. 2012 Sep;47(1–3):130–8. [<DOI>](#).
21. Igwe JC, Abia A, Ibeh C. Adsorption kinetics and intraparticulate diffusivities of Hg, As and Pb ions on unmodified and thiolated coconut fiber. *International Journal of Environmental Science & Technology*. 2008;5(1):83–92.

NOMENCLATURE

US	Ultrasound	C_1	constant of the intra particular diffusion model (mg/g)
AC	activated carbon	M	amount of adsorbent in industrial wastewater (g)
K_1	rate constant of pseudo-first- order sorption (min^{-1})	q	amount of metal ions adsorbed at time t,
K_2	rate constant of pseudo-first -order sorption (min^{-1})	q_e	amount of metal ions uptake at equilibrium per unit mass of adsorbent (mg/g)
K_L	Langmuir equilibrium constant (L/mg)	q_{max}	maximum monolayer adsorption capacity of the adsorbent (mg/g)
K_F	Freundlich constant((mg/g)/(mg/L) b_F)	R	coefficient of linear correlation
a_L	Langmuir constant (L/mg)	V	volume of wastewater
b_F	Freundlich exponent (dimensionless)	t	time (min)
C_0	initial metal ions concentration		
C	metal ions concentrations at time t		



Genetic Algorithm Based Nonlinear Optimization of Adsorption Processes

Dilek Özmen^{1*}  , Gülşen Fikir¹ 

¹Istanbul University-Cerrahpaşa, Dept. of Chemical Engineering, İstanbul, 34320, Turkey

Abstract: In this study, for different adsorption processes, nonlinear isotherm, kinetic model and thermodynamic parameters were calculated using genetic algorithm-based optimization method. Nonlinear equations were directly used as the model parameters can change to give false results when they are transformed to linear forms. Fifteen isotherms and two kinetic models were considered. All the experimental data was taken from the literature. Methylene green, thiram, and phenol red were used as the adsorbates and silica gel and chemically activated coal mining waste with potassium carbonate (K_2CO_3) or zinc chloride ($ZnCl_2$) were used as the adsorbents. For three different temperatures, the Root Mean Square Error (RMSE) values were obtained between calculated and the experimental data. The biggest RMSE values were obtained as 5.23×10^{-1} for Freundlich isotherm at 45 °C and the smallest RMSE value was obtained as 3.19×10^{-4} for Halsey isotherm at 35°C. For the kinetic study, Lagergren and Particle Internal Diffusion models were applied to the experimental data for three different initial concentrations and it was shown that Lagergren pseudo-first-order Kinetic Model fits better to experimental data. Thermodynamic calculations were made for two different initial pH values and four different temperatures. The Arrhenius factor (A) and Arrhenius activation energies (E_a) (kJ/mol) were also calculated.

Keywords: Adsorption, genetic algorithm, isotherms, kinetics, thermodynamics.

Submitted: October 13, 2021. **Accepted:** November 25, 2021.

Cite this: Özmen D, Fikir G. Genetic Algorithm Based Nonlinear Optimization of Adsorption Processes. JOTCSB. 2021;4(2):47-56.

***Corresponding author. E-mail:** dilekus@iuc.edu.tr.

INTRODUCTION

Separation can be specified as the process that transforms a mixture into two or more products that are compositionally different from each other. Separation is a challenging process; as it is the exact opposite of the common process called mixing, which is a process promoted by the second law of thermodynamics. Therefore, the steps of the separation process are the most costly steps in various industries like chemical, pharmaceutical, and petrochemical industries (1). Adsorption technology has a major share in the separation and purification processes that are the value-adding steps of the process industry. Adsorption is also a crucial element of the removal of unwanted components from wastewater and air streams (2). It has been known for over a century that some solids are able to remove color from solutions that contain dyes. Also, if the air that is contaminated with

unwanted odors is passed through charcoal, they can be eliminated. Despite the fact that such processes were not well comprehended until the early twentieth century, they represent the starting of the adsorption technology as a tool for the separation and purification of gases and liquids. Inarguably, adsorption process has been continuously advancing as competition processes like distillation and absorption have been advancing in time (3).

For most of the separation processes, the separation can happen in the presence of a mass separating agent. For adsorption, this mass agent is the adsorbent, or sorbent. Hence, the performance of any separation or purification process by adsorption is directly linked to the quality of the adsorbent, or sorbent (1). In this work, experimental data of studies investigating methylene green (BG5) adsorption with silica gel adsorption (4), thiram

adsorption with CMWZn, and adsorption of BG5 or phenol red sodium salt with CMWK adsorbent (5) were used. CMWK and CMWZn are adsorbents that are chemically activated coal mining waste with potassium carbonate (K_2CO_3) or zinc chloride ($ZnCl_2$), respectively. Nonlinear model solutions of the experimental data were used for calculations, and results compared with linear solutions given in the literature (4, 5). There are not many studies in the literature in which many isotherm models, thermodynamic, and kinetic parameters are examined together with experimental data and nonlinear and linear solutions are compared.

EXPERIMENTAL SECTION

Materials

The experimental data obtained using chemicals were listed in Table 1. Thiram in the adsorbates list in Table 1 is the most simple thiuram disulfide and the oxidized dimer of dimethyldithiocarbamate. Thiram is used as an ectoparasiticide to prevent fungal diseases in crops and seeds, as a fungicide

and as an animal repellent to protect the fruit trees and ornamentals against rabbits, deer and rodents.

Methylene green is a dye that is a heterocyclic aromatic chemical compound like methylene blue. It is used as a visible light-activated photocatalyst in organic synthesis. Phenol Red sodium salt is widely used as a pH indicator. Silica gel consists of an irregular tridimensional framework of interlacing oxygen and silicon atoms. It has pores and voids of nanometer-scale. It is a porous and amorphous form of silicon dioxide, or silica. The voids mentioned may be containing water or other liquids, or they may be filled with gas or vacuum. Silica gel is an efficient desiccant or drying agent as its high specific surface area which is around $800 \text{ m}^2/\text{g}$ makes it possible to adsorb the water instantly. The adsorbent used in kinetic studies were prepared from coal mining waste by chemical activation with $ZnCl_2$ and K_2CO_3 . In the text, these adsorbents are named as CMWZn and CMWK, respectively. The properties of the chemicals are described in more detail in the original literature (4, 5).

Table 1: The chemicals used for isotherm, kinetic and thermodynamic studies.

Study type	Adsorbents*	Adsorbates**	References
Isotherm	Silica gel	BG5	(4)
Kinetic	CMWZn	Thiram	(5)
Arrhenius equation	CMWK	BG5 or PRNa	(5)
Thermodynamics	CMWK	PRNa	(5)

*CMWK: Chemically activated coal mining waste with K_2CO_3 , CMWZn: Chemically activated coal mining waste with $ZnCl_2$.

**BG5: Methylene green, PRNa: Phenol Red sodium salt

Methods

Fifteen different isotherms, two kinetic models, and thermodynamic parameters using experimental adsorption data taken from literature were calculated using genetic algorithm-based optimization with non-linear solutions. All calculations of model parameters and error values were performed using MATLAB®. Since the experimental adsorption data obtained from the literature were calculated by linear optimization, the results with nonlinear solutions in this study are given comparatively.

The amount of molecule adsorbate per unit mass of adsorbent, that is, the equilibrium adsorption capacity of adsorption can be calculated using Eq. 1:

$$q_e = (C_0 - C_e) \times V / m \quad (1)$$

where q_e is the amount of adsorbate onto adsorbent (mg/g); C_0 and C_e (ppm) are the concentration of adsorbate at initial and equilibrium, respectively; V is the volume of solution (L) and m is the mass of the adsorbent (g) (4-6).

Adsorption Isotherms

To understand the basics of an adsorption process, one highly depends on the adsorption isotherm of the particular adsorption process. The analytical

forms of adsorption isotherm equations depend on the type of the surface phase that can be considered as a monolayer or multilayer, and as localized, mobile. Models mentioned here tend to be complex ones because of the energetic and structural heterogeneity of the adsorbent surfaces that are the main attributes of a many number of adsorbents used in the industry or in the laboratories. If a thermodynamic equilibrium relationship between the quantity of the adsorbed molecule by a unit mass of adsorbent and the amount of adsorbate remaining in the bulk fluid phase at a constant temperature and pH is assumed, various adsorption isotherm models can be derived (6). It is common knowledge that there are over 100 isotherm equations derived based on several mathematical, physical and experimental considerations. One can explain the differences by the fact that the different types of adsorption, solid-gas, solid-liquid and liquid-gas have different properties and hence, these differences should be discussed and explained with different physical pictures and mathematical treatments (7).

In this work, from the 2-parameter adsorption isotherm models, Jovanovich (mono-layer), Halsey (multi-layer), Temkin and Freundlich; from the 3-parameter adsorption isotherm models, Redlich-Peterson, Sips, Koble-Corrigan, Radke- Prausnitz, Fritz-Schlunder(III) (mono-layer) and Brunauer-

Emmett-Teller (BET), Aranovich (multi-layer) models; from the 4-parameter adsorption isotherm models, Fritz-Schlunder(IV), Baudu (mono-layer) and Guggenheim Anderson de-Boer (GAB), Anderson (IV) (multi-layer) models were studied. Root Mean Square Error (RMSE), one of the nonlinear error functions, was used to see the compatibility of nonlinear isotherm models with the experimental equilibrium data.

The error function calculated to justify the suitability of isotherm models to experimental data for

understanding the adsorption process, which is defined as Eq. (2) is the RMSE (6):

$$RMSE = \sqrt{\frac{1}{n} \sum_{j=1}^n (q_{e,exp} - q_{e,cal})^2} \quad (2)$$

where $q_{e,exp}$ and $q_{e,cal}$ are the amount of adsorption at equilibrium (mg/g) experimentally and calculated with models, respectively. n is the number of measurements. Smaller RMSE value indicates better fitness. For different temperatures, isotherm parameters and RMSE values are shown in Table 2.

Table 2: Monolayer or multilayer isotherm parameters and RMSE values calculated with nonlinear optimization for different temperatures.

	Isotherm Models*	Isotherm Parameters				RMSE
2 PARA METE RS	Freundlich	k_f	$1/n_f$	-	-	
	25°C	5.8482	1.5565	-	-	0.0475
	35°C	0.67	2.44	-	-	0.0327
	45°C	1.06	3.98	-	-	0.5229
	Jovanovich	q_{mJ}	K_j	-	-	
	25°C	-1,7891	-1.4511	-	-	0.0559
	35°C	-0.785	-0.759	-	-	0.1434
	45°C	-0.0037	-5.5	-	-	0.1584
	Temkin	B_T	A_T	-	-	
	25°C	2.6800	1.578	-	-	0.2646
	35°C	2.1086	1.499	-	-	0.0836
	45°C	1.5391	6.762	-	-	0.0959
	Halsey	K_H	m_H	-	-	
	25°C	0.312	-0.704	-	-	0.0004 6
	35°C	1.159	-0.437	-	-	0.0003 2
45°C	0.9867	-0.248	-	-	0.0695 0	
3 PARA METE RS	Redlich-Peterson	K_R	a_R	g	-	
	25°C	3.0066	-10.3	5.38	-	0.0588
	35°C	-3.42	-5.93	-1.08	-	0.0136
	45°C	-2.39	-3.36	-2.27	-	0.243
	Sips	q_{ms}	a_s	B_s	-	
	25°C	6.75	1.45	1.83	-	0.0303
	35°C	4.44	0.20	2.81	-	0.0488
	45°C	-0.86	-0.50	2.31	-	0.1304
	Koble-Corrigan	A	n_K	B	-	
	25°C	8.362	1.706	1.0232	-	0.0131

4 PARA METE RS	35°C	4.78	8.94	3.10	-	0.1675
	45°C	-2.73	-9.48	-4.7	-	0.1048
	Radke- Prausnitz	q_{mRPI}	K_{RPI}	m_{RPI}		
	25°C	6.49	3.87	-0.49	-	0.0116
	35°C	1.07	2.42	-1.76	-	0.0288
	45°C	0.80	-4.41	-2.40	-	0.1374
	BET^b	q_{mBET}	C_{BET}	C_s		
	25°C	0.88	1.66	-1.55	-	0.0408
	35°C	3.30	-38.50	0.58	-	0.0516
	45°C	0.74	0.95	0.10	-	0.2284
	Aranovich	q_{mAr}	C_{ar}	C_s		
	25°C	-2.86	-7.58	9.47	-	0.0327
	35°C	-0.86	-6.01	13.51	-	0.0408
	45°C	-0.32	48.64	-64.86	-	0.0702
	Fritz- Schlunder(III)	q_{mFS}	K_{FS}	m_{FS}		
	25°C	14.30	5.53	-0.43	-	0.0124
	35°C	9.887	0.76	-1.84	-	0.0700
	45°C	-5.29	0.85	-2.45	-	0.1403
	Fritz- Schlunder(IV)	C	a	D	B	
	25°C	7.02	1.63	9.61	65.78	0.1766
	35°C	2.80	2.76	2.77	0.79	0.0306
	45°C	-5.29	-5.20	-6.48	-7.53	0.0710
	Baudu	q_{mB}	b_0	x	y	
	25°C	6.82	0.59	-4.89	1.64	0.0289
35°C	1.52	0.88	-2.34	3.07	0.0199	
45°C	0.83	-14.25	5.95	5.99	0.0132	
GAB^c	q_{mG}	C_{GAB}	K_G	C_s		
25°C	0.85	-18.89	2.31	-19.7	0.0265	
35°C	0.30	3.92	-16.20	19.42	0.0396	
45°C	0.092	2.30	-20.88	-29.4	0.0909	
Anderson (IV)	$q_{mAn,4}$	$C_{an,4}$	C_s	j		
25°C	0.53	24.36	7.30	-2.81	0.0016	
35°C	4.21	-0.64	-8.15	-3.54	0.0031	
45°C	-1.25	-2.36	8.49	6.59	0.0522	

**Italic* ones are multi-layer isotherm models. ^bBET: Brunauer-Emmett-Teller, ^cGAB: The Guggenheim Anderson de-Boer.

Adsorption Thermodynamics

Adsorption is a mass transport marvel that enables the molecules to attach onto the surface of a solid. The thermodynamics behavior of an adsorption process can be examined through three various thermodynamic parameters; standard Gibbs free energy change (ΔG°), standard enthalpy change

(ΔH°), and standard entropy change (ΔS°) (8). In order to check the feasibility of the process and the spontaneity, an important tool is the thermodynamic parameters. ΔG° value provides the information about spontaneity and feasibility of chemical reaction. To determine ΔG° value, both ΔH° , and ΔS° factors are used (9). Valuable

information can be obtained once the thermodynamic parameters are correctly estimated; e.g. the negative values of ΔG° show a spontaneous and favorable process. As the ΔG° magnitude gets higher, the adsorption also gets more spontaneous and favorable. When the ΔH° values are negative, this is an exothermic process, whereas when the ΔH° values are positive, the process is endothermic. The magnitude of ΔH° gives an indication on the interactions that happen between the adsorbate and adsorbent. Physisorption, such as Van der Waals interactions, is usually lower than $20 \text{ kJ}\cdot\text{mol}^{-1}$, and electrostatic interaction ranges from 20 to 80 kJ/mol. Chemisorption bond strengths can vary from 80 to 450 kJ/mol. When it comes to the ΔS° , negative values indicate that the randomness decreases at the solid solution interface during the adsorption, and positive values indicate the possibility of some readjustments or structural changes in the adsorbate-adsorbent complex. Eventually, if ΔH° contributes more than the $T\Delta S^\circ$ to find negative values of ΔG° , the adsorption is an enthalpy controlled process; on contrary, if $T\Delta S^\circ$ contributes more than ΔH° , the adsorption is an entropy controlled process (10).

The change in free energy (ΔG°) of adsorption can be calculated in a way such that

$$\Delta G^\circ = -RT \ln k_{eq} \quad (3)$$

in which T is absolute temperature (Kelvin), R is the gas constant (8.314 J/mol K) and K_e is the

equilibrium thermodynamic constant. The relationship of ΔG° with ΔH° and ΔS° can be written as

$$\Delta G^\circ = \Delta H^\circ - T \Delta S^\circ \quad (4)$$

If Eq. (3) is inserted into Eq. (4), it becomes

$$\ln k_{eq} = \frac{\Delta S^\circ}{R} - \frac{\Delta H^\circ}{R} \frac{1}{T} \quad (5)$$

Following this, the values of ΔH° and ΔS° can be found by the plot of $\ln(k_e)$ versus $(1/T)$. The graph is called the Van't Hoff plot. Many studies have used this methodology to estimate the adsorption thermodynamic parameters (10, 11).

It is rather easy to use the Van't Hoff plot but it is very important to precisely calculate the k_e which is the equilibrium thermodynamic constant. Actually, if you look at the literature, you can see different ways of calculating the k_e values, and unfortunately some do not make sense. As an example, in most cases, units are used with k_e ; however, from the mathematical viewpoint, a parameter that has a dimension cannot be computed logarithmically. The parameter in transcendental functions must be dimensionless; otherwise, the computation for this parameter is unreasonable (10). Therefore, the parameters were calculated using a nonlinear form of Eq. (5). The thermodynamic parameters (ΔH° , ΔG° , ΔS°) are shown in Table 3.

Table 3: Comparison of Thermodynamic Data Obtained at Different pH (Adsorbates: Phenol Red sodium salt, Adsorbents: CMWK*).

	pH=4.5		pH=8	
	This study	from Ref. (5)	This study	from Ref. (5)
ΔH° (J/mol)	-18657	-17709	16212	-15297
ΔS° (J/mol.K)	-46.22	-43.10	56.87	53.92
ΔG° (J/mol) at 20°C	-5178	-5081	-644	-500
ΔG° (J/mol) at 30°C	-4560	-4652	-982	-1040
ΔG° (J/mol) at 40°C	-4164	-4219	-1431	-1579
ΔG° (J/mol) at 50°C	-3894	-3788	-2202	-2118
RMSE	0.1833	0.1974	0.0623	0.0657

*CMWK: Chemically activated coal mining waste with K_2CO_3

Adsorption Kinetics

To be able to develop sorption kinetics, one needs to know the rate law that describes the sorption system. The rate law is determined by experimentation of the overall chemical reaction equation. There are three main requirements to the rate law:

- Knowing all the molecular details of the reaction, including the energetics and the stereo chemistry.

- Angles and interatomic distances throughout the course of the reaction.

- The individual molecular steps involved in the mechanism (12).

Similar approaches are used to study the adsorption kinetics and thermodynamics. The only difference is the analysis in the adsorbate concentration change over time (11). There are essentially three stages in the adsorption processes:

1. Diffusion across the liquid film surrounding the adsorbent particles, i.e., film diffusion or external diffusion;
2. Diffusion in the liquid contained in the pores and / or along the pore walls, which is called internal diffusion or intra-particle diffusion; and
3. Adsorption and desorption between the adsorbate and active sites, i.e., mass action.

One or more of these stages may have an effect on the adsorption rate. Various models have been proposed to find out which or which of these control the adsorption rate. To test the experimental data for the examination of the controlling mechanisms of the adsorption process, several kinetics models can be used. Some examples of these processes are chemical reaction, diffusion control, and mass transfer (13). Two different kinetic models are studied here: Lagergren Equation (pseudo-first-order kinetic model) and Weber-Morris intra-particle diffusion model.

Lin and Wang (14) prove that the best-fitting nonlinear forms of the kinetic models were better performing than the linear forms. The model parameters may be distorted when the nonlinear equations were transformed to linear forms. Therefore, nonlinear methods have been adopted to obtain the adsorption parameters.

Lagergren pseudo-first-order kinetic model

The first-order kinetics only describes the sorption sites and not the adsorption process as a whole (15). Bhattacharya and Venkobachar (16) presented a simple first order reversible kinetic model that has been applied to several other sorption systems (12, 16). In the pseudo-first-order kinetic model, it is assumed that the rate of occupation of sorption sites is proportional to the number of unoccupied sites (13).

$$q_t = q_e (1 - e^{-k_1 t}) \quad (6)$$

where q_t and q_e are the amount of adsorption at time t and at equilibrium (mg/g), consequently, and k_1 is the Lagergren rate constant (1/min) (17).

Figure 1 shows pseudo-first-order kinetic model curves in different initial concentrations. In Table 4, kinetic model parameters, k_1 , q_e , and RMSE values are given together with linear and non-linear solutions.

Weber-Morris intra-particle diffusion model

Weber and Morris considered only diffusion aspects, but they did not consider how transient adsorption of the adsorbate during the process might be anticipated to change the effective value of the diffusion coefficient D . Since sorption is a fast and non-limiting step in the adsorption process, the adsorption rate can be limited by film diffusion or/and intra-particle diffusion. According to intra-

particle diffusion, the uptake changes almost proportionally with the half power of time, $t^{0.5}$. The governing equation can be expressed as (18-20);

$$q_t = k_{id} t^{0.5} + C \quad (7)$$

where k_{id} is the intra-particle diffusion rate constant (mg/g. min^{0.5}), which can be evaluated from the slope of the linear plot of q_t versus $t^{0.5}$ and the intercept of the plot reveals C . The C (mg/g) values provide information about the thickness of the boundary layer (17, 19, 21, 22). Figure 2 shows nonlinear Weber-Morris plots in different initial concentrations. Model parameters, k_{id} and C , obtained by the linear and nonlinear method, are given in Table 4 together with the RMSE values obtained for the model.

Calculation and analysis of the activation energy

Activation energy is an important parameter that helps illuminate the mechanism formed for the adsorption process (18, 23). The rate constant of the adsorption is expressed as a function of temperature by the Arrhenius type relationship:

$$k = A \cdot e^{(-E_a/RT)} \quad (8)$$

where E_a is the Arrhenius activation energy (kJ/mol), A the Arrhenius factor, R the gas constant (8.314 J/mol K) and T is the solution temperature in Kelvin. The vastitude of activation energy is an indication on the type of adsorption that is mainly chemical or physical. The physisorption processes generally have energies in the range of 5–40 kJ/mol while higher activation energies (40–800 kJ/mol) suggest chemisorption (18, 24). At a certain temperature, the greater the activation energy, the slower the reaction; and the smaller the activation energy, the faster the reaction. In room temperature, if the activation energy calculated is less than 40 kJ/mol the rate of the reaction is quick; if it is greater than 120 kJ/mol, the rate of the reaction is rather slow (23). The data in Table 4 (or Figure 1 and 2) states that the adsorption process is in more accordance with the pseudo-first order kinetic model. So, for this reaction, the apparent activation energy is calculated by the coefficient of k_1 in pseudo-first order kinetic model. Since the calculated E_a values for the systems studied are less than 40 kJ/mol, one can say that the adsorption process is a rapid physical absorption process. The calculated activation energies (E_a), the Arrhenius factors (A) and RMSE values are given in Table 5 with comparison with the linear and non-linear solutions.

Genetic algorithm

Genetic algorithm is a heuristic search algorithm. It is evoked by the biological evolution process and is used to find the solution of the optimization problems. The algorithm starts with a set of

possible solutions called population and these populations are represented by chromosomes. A well-known application of the genetic algorithm is function optimization. The genetic algorithm contains the basic three operators called mutation, crossover and selection. Mutation randomly changes some of the gene values in a chromosome to create new gene values for better solutions. Crossover operator randomly mixes two distinct solutions' parts to obtain new solutions. Selection operator selects some chromosomes from the population for reproduction. (25).

A simple genetic algorithm steps are as follows (26):

- I. Start with candidate solutions to a problem (randomly generate initial population).
- II. Create new populations according to the following steps:
 - Calculate fitness function values for each solution in the population (raw fitness)
 - a) Select parents based on fitness values.
 - b) Choose elite members and pass to the next generations.
 - c) Produce children from the parents using mutation and crossover operators.
 - d) Replace the current population with the children to create the next generation.

In this study population size was selected 10000 for all calculations. The algorithm was stopped when the number of the iteration reached the value of 1000. While F_M shows the model function, the following Sum Square Error (SSE) fitness function is minimized using the genetic algorithm to find the model parameters.

$$\sum_{i=1}^n (y_i - F_M(x_i; \theta))^2 \quad (9)$$

where y and x are experimentally determined values, n is the number of the experimental data and θ is the model parameter vector.

RESULTS AND DISCUSSION

Table 1 listed the chemicals used for isotherm and kinetic studies the literature from which they were

taken. The equilibrium adsorption isotherms are crucial data to understand the adsorption mechanism. In this work, the two, three, and four parameter equilibrium adsorption isotherm models related to monolayer or multilayer adsorption were investigated; while in the original publications where experimental data were taken, only 3 isotherm models were used with their linear forms. In Table 2, isotherm parameters calculated for different temperatures and RMSE values are also given. The smallest error values were 4.6×10^{-4} (Halsey isotherm), 3.19×10^{-4} (Halsey isotherm) and 1.32×10^{-2} (Baudu isotherm) for 25, 35, and 45°C, respectively. The biggest RMSE values are 1.77×10^{-1} ; 1.68×10^{-1} and 5.23×10^{-1} . These values are for Fritz-Schlunder (IV) for 25°C, Koble-Corrigan isotherms for 35°C and Freundlich isotherm 45°C, respectively.

Figure 1 and 2 show the Lagergren pseudo-first order kinetic and Weber-Morris Intra-Particle Diffusion plots according to different initial concentrations, respectively. The thermodynamic parameters (ΔH° , ΔG° , ΔS°) were given in Table 3. When the pH value was increased from 4.5 to 8, the thermodynamic parameters also increased. Kinetic model parameters and activation energies calculated in comparison with linear and nonlinear solutions are given in Tables 4 and 5, respectively.

In the literature, in most cases, the pseudo-first order equation of Lagergren is usually applicable over the first 20-30 minutes of the sorption process as it does not work well for the whole range of contact time (27). For thiram adsorption using CMWZn, adsorption time is determined as 36 min (5). Therefore, appropriate results were obtained for the Lagergren pseudo-first order kinetic model. For the non-linear solutions, RMSE values are between 0.2345 and 0.3112, nonlinear RMSE values are between 0.3057 and 0.5334. The RMSE values for the Weber-Morris Intra-Particle Diffusion model are 0.3204 and 0.7429 for $C_0 = 8$ mg/L and $C_0 = 14$ mg/L, respectively. These values are the same for both linear and nonlinear solutions.

CONCLUSION

In this study, codes that are written with genetic algorithm based optimization have been used to calculate 15 isotherm models and 2 kinetic models using experimental adsorption data from the literature. The values calculated with these codes are presented by comparing them with the values in the original publications. While 15 isotherm models are given in this study, since only 2 or 3 isotherm models are used in original publications, only non-linear solutions are given in Table 2. RMSE (Root Mean Square Error) values calculated for non-linear solutions are already quite low values. The error values were calculated using MATLAB®, too. The fact that the RMSE value is close to zero is a sign of the model and its compatibility with the experimental data. Small RMSE values obtained by using the genetic algorithm with nonlinear solutions are a sign that the applied solution is more suitable than linear solutions.

Since the charge intensities and therefore the electrostatic interactions of the adsorbent and adsorbed substances will change depending on the pH value of the environment, the pH of the environment has a great effect on the adsorption. At pH=8, the enthalpy change (ΔH°) was found as positive value (endothermic) with nonlinear equations, but it was found as negative value (exothermic) with linear equations. As it can be understood, the use of nonlinear forms of the equations is important to understand the nature of adsorption processes.

For the kinetic study, Lagergren pseudo-first order kinetic model and Weber-Morris Intra-Particle Diffusion model were applied to the experimental data obtained for three different initial concentrations obtained from the literature. Tables 4 and 5 show that the error values obtained for nonlinear solutions are smaller when compared to linear solutions, except for the Weber-Morris kinetic model.

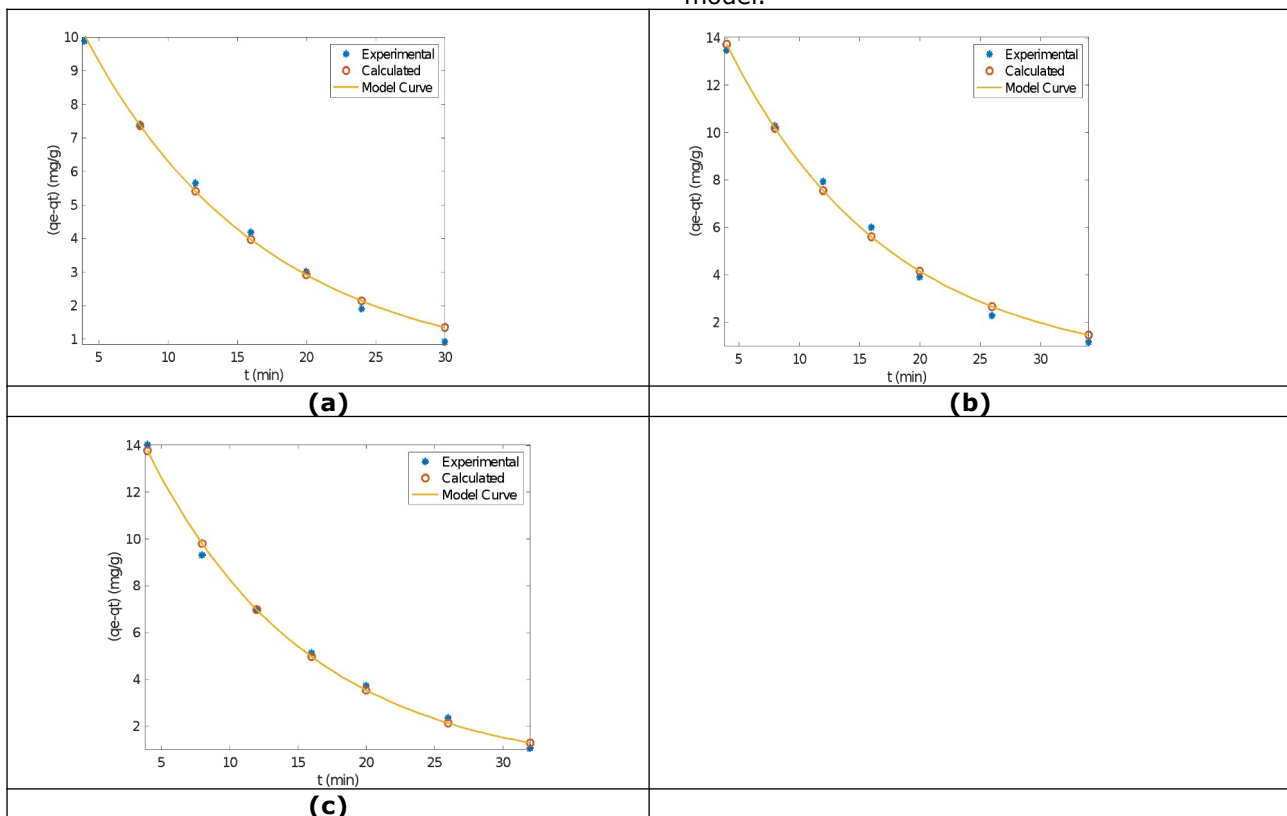


Figure 1: Lagergren pseudo-first-order Kinetic Model curves in different initial concentrations (a) $C_0 = 8$ mg/L (b) $C_0 = 10$ mg/L (c) $C_0 = 14$ mg/L.

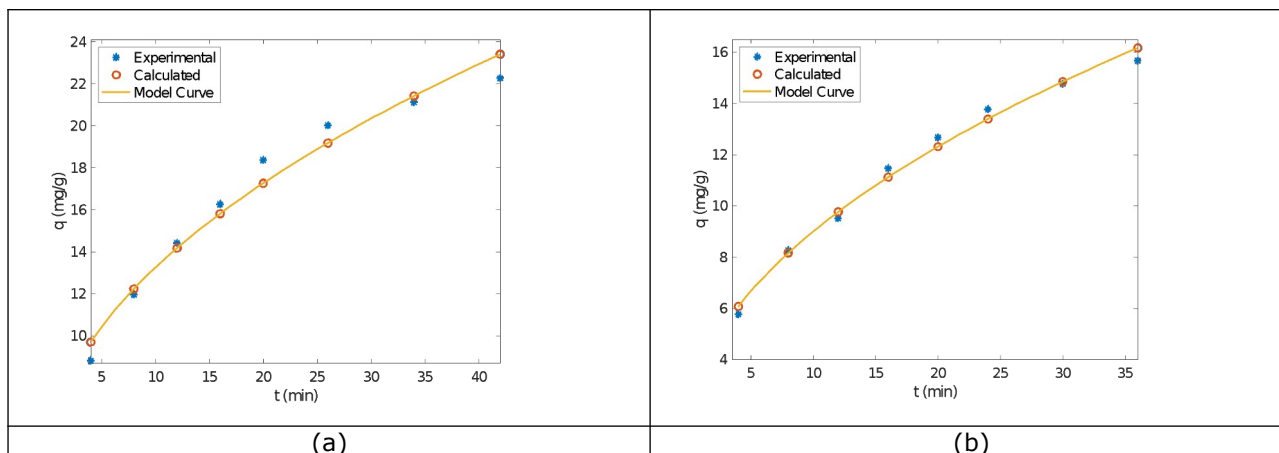


Figure 2: The Weber-Morris Intra-Particle Diffusion kinetic model curves in different initial concentrations (a) $C_0 = 8 \text{ mg/L}$ (b) $C_0 = 14 \text{ mg/L}$.

Table 4: Comparison of model parameters, linear and nonlinear solutions obtained for Lagergren and Weber-Morris kinetic models.

	$C_0 = 8 \text{ mg/L}$		$C_0 = 10 \text{ mg/L}$		$C_0 = 14 \text{ mg/L}$	
	nonlinear	Linear*	nonlinear	Linear*	nonlinear	Linear*
<i>Lagergren pseudo-first-order kinetic model</i>						
k_1 (1/min)	0.077	0.090	0.085	0.088	0.075	0.084
q_e (mg/g)	13.66	15.83	19.33	20.11	18.50	20.45
RMSE	0.2345	0.5217	0.2553	0.3057	0.3112	0.5334
<i>Weber-Morris Intra-Particle Diffusion kinetic model</i>						
k_{id} (mg/g.min ^{-1/2})	2.5222	2.5252	-	-	3.0583	3.0561
C (mg/g)	1.0219	1.0087	-	-	3.5735	3.5827
RMSE	0.3204	0.3204	-	-	0.7429	0.7429

*from Ref. (5)

Table 5: The Arrhenius factor (A) and Arrhenius activation energy (E_a) (kJ/mol) calculated with RMSE values for different systems.

Adsorbates: Methylene Green Adsorbents: CMWK*	pH=5		pH=8	
	nonlinear	linear	nonlinear	linear
A	549.6	482.992	0.0091	0.007
E_a (kJ/mol)	13.884	13.552	-17.576	-18.125
RMSE	0.0693	0.0702	0.1661	0.1786
Adsorbates: Phenol Red sodium salt Adsorbents: CMWK*	pH= 4.5		pH=8	
A	0.0039	0.006	934.8	655.239
E_a (kJ/mol)	-18.657	-17.709	16.212	15.298
RMSE	0.1833	0.1974	0.0623	0.0657

*CMWK: Chemically activated coal mining waste with K_2CO_3

CONFLICT OF INTEREST

The authors have declared no conflict of interest.

ACKNOWLEDGMENTS

This work was a part of the project supported by the Scientific Research Projects Coordination Unit of

Istanbul University. Project number YADOP/10662 and 55671.

REFERENCES

1. Yang RT. Adsorbents: fundamentals and applications. Hoboken, N.J: Wiley-Interscience; 2003. 410 p. ISBN: 978-0-471-29741-3.

2. Aarden FF. Adsorption onto heterogeneous porous materials: equilibria and kinetics [Internet] [PhD Thesis]. [Eindhoven, the Netherlands]: Technische Universiteit Eindhoven; 2001 [cited 2021 Nov 25]. [<URL>](#).
3. Thomas WJ, Crittenden BD. Adsorption technology and design. Oxford ; Boston: Butterworth-Heinemann; 1998. 271 p. ISBN: 978-0-7506-1959-2.
4. Topçuoğlu E. Boyar maddelerin çeşitli adsorbanlarla adsorpsiyonunun incelenmesi [MSc Thesis]. [Istanbul, Turkey]: Istanbul University; 2016.
5. Mısırlı T. Kömür Madeni Atıklarından Elde Edilen Adsorbentlerle Boyar Madde ve Pestisit Uzaklaştırılması [MSc Thesis]. [Istanbul, Turkey]: Istanbul University; 2004.
6. Saadi R, Saadi Z, Fazaeli R, Fard NE. Monolayer and multilayer adsorption isotherm models for sorption from aqueous media. Korean J Chem Eng. 2015 May;32(5):787–99. [<DOI>](#).
7. Tóth J, editor. Adsorption: theory, modeling, and analysis. New York: Marcel Dekker; 2002. 878 p. (Surfactant science series). ISBN: 978-0-8247-0747-7.
8. Chattaraj S, Mohanty D, Kumar T, Halder G. Thermodynamics, kinetics and modeling of sorption behaviour of coalbed methane – A review. Journal of Unconventional Oil and Gas Resources. 2016 Dec;16:14–33. [<DOI>](#) .
9. Siddiqui SI, Chaudhry SA. A review on graphene oxide and its composites preparation and their use for the removal of As³⁺ and As⁵⁺ from water under the effect of various parameters: Application of isotherm, kinetic and thermodynamics. Process Safety and Environmental Protection. 2018 Oct;119:138–63. [<DOI>](#).
10. Bonilla-Petriciolet A, Mendoza-Castillo DI, Reynel-Ávila HE, editors. Adsorption Processes for Water Treatment and Purification. 1st ed. 2017. Cham: Springer International Publishing : Imprint: Springer; 2017. 1 p. ISBN: 978-3-319-58136-1.
11. Cherkasov N. Liquid-phase adsorption: Common problems and how we could do better. Journal of Molecular Liquids. 2020 Mar;301:112378. [<DOI>](#).
12. Ho YS, McKay G. Pseudo-second order model for sorption processes. Process Biochemistry. 1999 Jul;34(5):451–65. [<DOI>](#).
13. Ghasemi M, Ghasemi N, Zahedi G, Alwi SRW, Goodarzi M, Javadian H. Kinetic and equilibrium study of Ni(II) sorption from aqueous solutions onto Peganum harmala-L. Int J Environ Sci Technol. 2014 Oct;11(7):1835–44. [<DOI>](#).
14. Lin J, Wang L. Comparison between linear and non-linear forms of pseudo-first-order and pseudo-second-order adsorption kinetic models for the removal of methylene blue by activated carbon. Front Environ Sci Eng China. 2009 Sep;3(3):320–4. [<DOI>](#).
15. Doğan M, Alkan M. Adsorption kinetics of methyl violet onto perlite. Chemosphere. 2003 Jan;50(4):517–28. [<DOI>](#).
16. Bhattacharya AK, Venkobachar C. Removal of Cadmium (II) by Low Cost Adsorbents. Journal of Environmental Engineering. 1984 Feb;110(1):110–22. [<DOI>](#).
17. Aljeboree AM, Alshirifi AN, Alkaim AF. Kinetics and equilibrium study for the adsorption of textile dyes on coconut shell activated carbon. Arabian Journal of Chemistry. 2017 May;10:S3381–93. [<DOI>](#).
18. Guo Z, Liu X, Huang H. Kinetics and Thermodynamics of Reserpine Adsorption onto Strong Acidic Cationic Exchange Fiber. Peters M, editor. PLoS ONE. 2015 Sep 30;10(9):e0138619. [<DOI>](#).
19. Idan IJ, Abdullah LC, Choong TS, Jamil SNABM. Equilibrium, kinetics and thermodynamic adsorption studies of acid dyes on adsorbent developed from kenaf core fiber. Adsorption Science & Technology. 2018 Feb;36(1–2):694–712. [<DOI>](#).
20. Hubbe M, Azizian S, Douven S. Implications of apparent pseudo-second-order adsorption kinetics onto cellulosic materials: A review. BioRes. 2019 Aug;14(3):7582–626. [<DOI>](#).
21. Singh SK, Townsend TG, Mazyck D, Boyer TH. Equilibrium and intra-particle diffusion of stabilized landfill leachate onto micro- and meso-porous activated carbon. Water Research. 2012 Feb;46(2):491–9. [<DOI>](#).
22. Abdel Salam M, Burk RC. Thermodynamics and Kinetics Studies of Pentachlorophenol Adsorption from Aqueous Solutions by Multi-Walled Carbon Nanotubes. Water Air Soil Pollut. 2010 Jul;210(1–4):101–11. [<DOI>](#).
23. Chen F, Zhou C, Li G, Peng F. Thermodynamics and kinetics of glyphosate adsorption on resin D301. Arabian Journal of Chemistry. 2016 Nov;9:S1665–9. [<DOI>](#).
24. Hameed BH, Ahmad AA, Aziz N. Isotherms, kinetics and thermodynamics of acid dye adsorption on activated palm ash. Chemical Engineering Journal. 2007 Sep;133(1–3):195–203. [<DOI>](#).
25. Mitchell M. An introduction to genetic algorithms. Cambridge, Mass: MIT Press; 1996. 205 p. (Complex adaptive systems). ISBN: 978-0-262-13316-6.
26. Anonymous. How the Genetic Algorithm Works [Internet]. [cited 2021 Oct 13]. [<URL>](#).
27. Ho YS, McKay G. Kinetic Models for the Sorption of Dye from Aqueous Solution by Wood. Process Safety and Environmental Protection. 1998 May;76(2):183–91. [<DOI>](#).